

# H3K56 acetylation regulates chromatin maturation following DNA replication

Received: 11 July 2024

Accepted: 2 December 2024

Published online: 02 January 2025

 Check for updates

Shoufu Duan  <sup>1,2</sup> , Ilana M. Nodelman  <sup>3</sup>, Hui Zhou <sup>1</sup>, Toshio Tsukiyama <sup>4</sup>, Gregory D. Bowman  <sup>3</sup> & Zhiguo Zhang  <sup>1</sup> 

Following DNA replication, the newly reassembled chromatin is disorganized and must mature to its steady state to maintain both genome and epigenome integrity. However, the regulatory mechanisms governing this critical process remain poorly understood. Here, we show that histone H3K56 acetylation (H3K56ac), a mark on newly-synthesized H3, facilitates the remodeling of disorganized nucleosomes in nascent chromatin, and its removal at the subsequent G2/M phase of the cell cycle marks the completion of chromatin maturation. *In vitro*, H3K56ac enhances the activity of ISWI chromatin remodelers, including yeast ISWI and its human equivalent SNF2h. *In vivo*, a deficiency of H3K56ac in nascent chromatin results in the formation of closely packed di-nucleosomes and/or tetra-nucleosomes. In contrast, abnormally high H3K56ac levels disrupt chromatin maturation, leading to genome instability. These findings establish a central role of H3K56ac in chromatin maturation and reveal a mechanism regulating this critical aspect of chromosome replication.

Chromatin, an organized complex of DNA, RNA and proteins, encodes epigenetic information and maintains genome integrity. The basic repeating unit of chromatin is the nucleosome, consisting of ~146 base-pairs of DNA wrapped around a histone octamer, comprised of one histone (H3-H4)<sub>2</sub> tetramer and two histone H2A-H2B dimers<sup>1</sup>. Chromatin is further separated into different functional domains, each with distinct modified forms of histones. During DNA replication, chromatin structures are transiently disassembled to allow DNA replication machinery to replicate nucleosomal DNA. Following passage of the replication fork, chromatin structures must be restored to their original states to maintain genome integrity and cell identity<sup>2–6</sup>. In recent years, it has become increasingly clear that alterations in chromatin structures drive tumorigenesis in many organs<sup>7–12</sup>, highlighting the importance to restore chromatin structures following DNA replication.

The restoration of chromatin structures starts with the assembly of replicated DNA into nucleosomes using both parental histones and newly-synthesized histones in a process tightly coupled with ongoing

DNA synthesis<sup>4,6</sup>. Recent studies show that parental (H3-H4)<sub>2</sub> tetramers, the primary carriers of epigenetic modifications, are equally distributed to leading and lagging strands of DNA replication forks<sup>13–15</sup>. Moreover, these parental histones can remember their positions along DNA<sup>16,17</sup>. Furthermore, several components of the replisome bind parental histones and facilitate the transfer of parental histones to leading and lagging strands of DNA replication forks. Specifically, Dpb3-Dpb4, two subunits of leading strand DNA polymerase Pol ε, facilitate the transfer of parental histones to leading strands of DNA replication forks<sup>13</sup>. On the other hand, Mcm2-Ctf4-Polo<sup>18</sup> and PCNA-Pol delta<sup>19</sup> are important for the transfer of parental (H3-H4)<sub>2</sub> to lagging strands. In cells containing mutations in Mcm2, Dpb3 and Dpb4, parental and newly synthesized histones are asymmetrically distributed at leading and lagging strands. However, it was not known whether this asymmetric distribution of parental and newly synthesized histones affects the subsequent chromatin maturation at leading and lagging strands in mutant cells.

<sup>1</sup>Institute for Cancer Genetics, Department of Pediatrics and Department of Genetics and Development, Columbia University Irving Medical Center, New York, NY 10032, USA. <sup>2</sup>State Key Laboratory of Mycology, Institute of Microbiology, Chinese Academy of Sciences, Beijing 100101, China. <sup>3</sup>Thomas C. Jenkins Department of Biophysics, Johns Hopkins University, Baltimore, MD 21218, USA. <sup>4</sup>Basic Sciences Division, Fred Hutchinson Cancer Center, Seattle, WA 98109, USA.  e-mail: [duansf@im.ac.cn](mailto:duansf@im.ac.cn); [zz2401@cumc.columbia.edu](mailto:zz2401@cumc.columbia.edu)

Newly synthesized histone H3-H4, with modifications distinct from parental histones, are deposited by histone chaperones including CAF-1 and Asf1<sup>4,6,20</sup>. A combination of genetic, biochemical, and structural-biology approaches support the following model of nucleosome assembly of new H3-H4 in budding yeast<sup>21-27</sup>. First, new H3-H4 form the Asf1-H3-H4 heterotrimeric complex. Asf1 then presents H3-H4 to the lysine acetyltransferase Rtt109 for acetylation of H3 lysine 56 (H3K56ac)<sup>27-30</sup>. Histone chaperone CAF-1 and Rtt109 bind preferentially H3K56ac-containing tetramers for nucleosome formation<sup>21,22,24,31-33</sup>. Once assembled into nucleosomes, H3K56ac is removed by Hst3 and Hst4, two members of the Sir2 family of NAD-dependent histone acetylases, during late S and G2/M phase of the cell cycle<sup>34,35</sup>. Yeast cells lacking Hst3 and Hst4 are sensitive to a variety of DNA damage agents, highlighting the importance of removing this mark following DNA replication. However, it is not known why abnormally high H3K56ac levels in Hst3 and Hst4 mutant yeast cells cause genome instability.

Nucleosomes formed soon after DNA replication are not uniformly spaced. Furthermore, it has been shown that newly formed nucleosomes can replace transcription factors as well as other chromatin binding proteins and disrupt chromatin landscape<sup>36</sup>. Therefore, the initially disorganized nucleosomes must adopt the positions of steady state chromatin in a process called chromatin maturation. In both budding yeast and mammalian cells, chromatin at different chromatin loci mature with variable kinetics. For instance, genes with rapid maturation kinetics are enriched with specific histone modifications including H3K4me3 and H4K12ac and the histone variant H2A.Z. There are reports indicating that transcription levels affect the rate of nucleosome maturation, but the exact mechanism remains under debate. For instance, some studies have shown that nucleosomes at lowly expressed genes mature at a faster rate than those at highly expressed genes<sup>36,37</sup>. Conversely, other studies suggest that nucleosomes in highly transcribed regions mature more quickly than those in lowly expressed regions<sup>38</sup>. These results highlight the challenges of studying chromatin maturation following DNA replication. Therefore, it has been largely unexplored how chromatin maturation following DNA replication is regulated.

ATP-dependent chromatin remodelers can change the position, composition, and occupancy of the histone core on DNA<sup>39-42</sup>. The four most extensively chromatin remodeler subfamilies are imitation switch (ISWI), chromodomain helicase DNA-binding (CHD), switch-sucrose non-fermentable (SWI/SNF), and INO80. Among them, ISWI and CHD family chromatin remodelers have been implicated in chromatin assembly in yeast and mammalian cells. In vitro, CHD1 and the ISWI remodeler ACF promote the formation of regularly spaced nucleosome in collaboration with histone chaperone Nap1<sup>43-45</sup>. Furthermore, nucleosomal intermediates formed in these in vitro reactions resemble nascent chromatin. In budding yeast cells, Chd1 and Isw1 are required for establishing arrays of regularly phased nucleosomes near transcription start sites (TSS)<sup>46-48</sup>. Cells lacking both Isw1 and Chd1 show weakly phased and irregularly spaced nucleosomes, and a propensity to form closely-packed di-nucleosomes at transcription starting sites. In vitro, the Isw1a chromatin remodeler, consisting of Isw1 and loc3, prefers to mobilize di-nucleosomes over mono-nucleosomes<sup>49</sup>. In mammalian cells, it has been shown that SNF2h (SMARCA5) is important to regulate nucleosome repeat length at G1/S and during S phase of the cell cycle<sup>50</sup>. Most of these in vivo studies focus on the role of Isw1 and Chd1 in gene transcription. It is not known whether or how Chd1 and ISWI remodelers may participate in maturation of chromatin in newly replicated DNA. Importantly, it is largely unknown whether and how histone modifications in nascent chromatin, which include modifications on parental and newly synthesized histones, might help direct chromatin maturation.

Here we report that nascent chromatin following DNA replication requires H3K56ac, a mark on newly synthesized histone H3, for proper

nucleosome spacing. In *mcm2-3A* and *dpb3Δ* cells, which have shown the asymmetric distribution of new histones at lagging and leading strands due to defects in the transfer of parental histones to lagging and leading strands, respectively, we found the asymmetric distribution of closely packed nucleosomes at replicating DNA strands. We show that the resolution of these closely-packed nucleosomes in nascent chromatin in vivo is assisted by the Isw1 remodeler, and that the H3K56ac stimulates Isw1 remodeling in vitro. Remarkably, H3K56ac removal after S phase facilitates chromatin maturation and genome stability.

## Results

### Di-nucleosome-and tetra-nucleosome-sized fragments at nascent chromatin of leading and lagging strands in *mcm2-3A* and *dpb3Δ* cells are asymmetrically distributed

To study nucleosome dynamics in nascent chromatin, we used MNase, an endo- and exo-nuclease that cleaves the naked DNA between nucleosomes, releasing the nucleosomes from chromatin, to map nucleosome positions and occupancy<sup>51</sup>. Briefly, we released G1-arrested yeast cells into a medium containing bromodeoxyuridine (BrdU) to label newly synthesized DNA. Following MNase digestions, we performed BrdU immunoprecipitation to enrich newly synthesized DNA followed by strand-specific (ss) sequencing (BrdU-IP-ssSeq). In this way, we could monitor nucleosome dynamics at leading and lagging strands at nucleotide resolution (Supplementary Fig. 1a). In this study, the optimal MNase digestion (4U) generated a DNA ladder with the majority of DNA as mono- and di-nucleosomes (Supplementary Fig. 1b). Compared to input samples at G1 phase, nucleosomes at nascent chromatin were less well organized based on analysis of nucleosome occupancy and positioning surrounding DNA replication origins, transcription starting sites, and +1 nucleosomes of genes within replicated regions (Supplementary Fig. 1c-e). These results are consistent with previous findings that nucleosomes formed soon after replication are irregularly organized<sup>36</sup>.

Based on analysis of the distribution of parental histones (H3K4me3) and newly synthesized histones (H3K56ac) at replicating DNA strands using eSPAN<sup>52</sup>, we have shown previously that H3K4me3 and H3K56ac were equally distributed at leading and lagging strands in wild type cells<sup>13,18</sup>. In contrast, H3K4me3 and H3K56ac are asymmetrically distributed at leading and lagging strands in *mcm2-3A* and *dpb3Δ* mutant cells (see also Fig. 1b, bottom two panels). Therefore, we compared nucleosome occupancy and positioning in nascent chromatin in wild type, *mcm2-3A*, and *dpb3Δ* mutant cells. We found that the occupancy of mono-nucleosomes around replicated genes between wild type and each mutant cells exhibited a similar distribution pattern, albeit with a slightly decreased-occupancy in *mcm2-3A* or *dpb3Δ* cells compared to wild type cells (Supplementary Fig. 1f-h).

We then separated sequence reads of BrdU-IP-ssSeq into two different groups, mono-nucleosome (120-200 bp) and di-nucleosome (250-400 bp) size fragments, and used the formula  $(W - C)/(W + C)$  to calculate the relative abundance of mono-nucleosomes and di-nucleosomes at leading and lagging strands (Fig. 1a). In wild type cells, BrdU-IP-ssSeq bias calculated using with mono-nucleosome or di-nucleosome sized fragments showed no bias towards either leading and lagging strands, suggesting that equal amounts of mono- and di-nucleosomes were released from leading and lagging strands upon MNase digestion (Fig. 1b, c). In *mcm2-3A* and *dpb3Δ* cells, almost equal amounts of mono-nucleosomes were also released from leading and lagging strands upon MNase digestion (Fig. 1b-d). Surprisingly, BrdU-IP-ssSeq bias calculated using di-nucleosome-sized DNA fragments exhibited a strong leading and lagging strand bias in *mcm2-3A* and *dpb3Δ* cells, respectively (Fig. 1b-d) based on the analysis of BrdU-IP-ssSeq signals at each of the 134 early-firing origins (Fig. 1c) as well as the average bias signals of all fired origins (Fig. 1d). These results indicate that more di-nucleosomes were formed leading strand than lagging

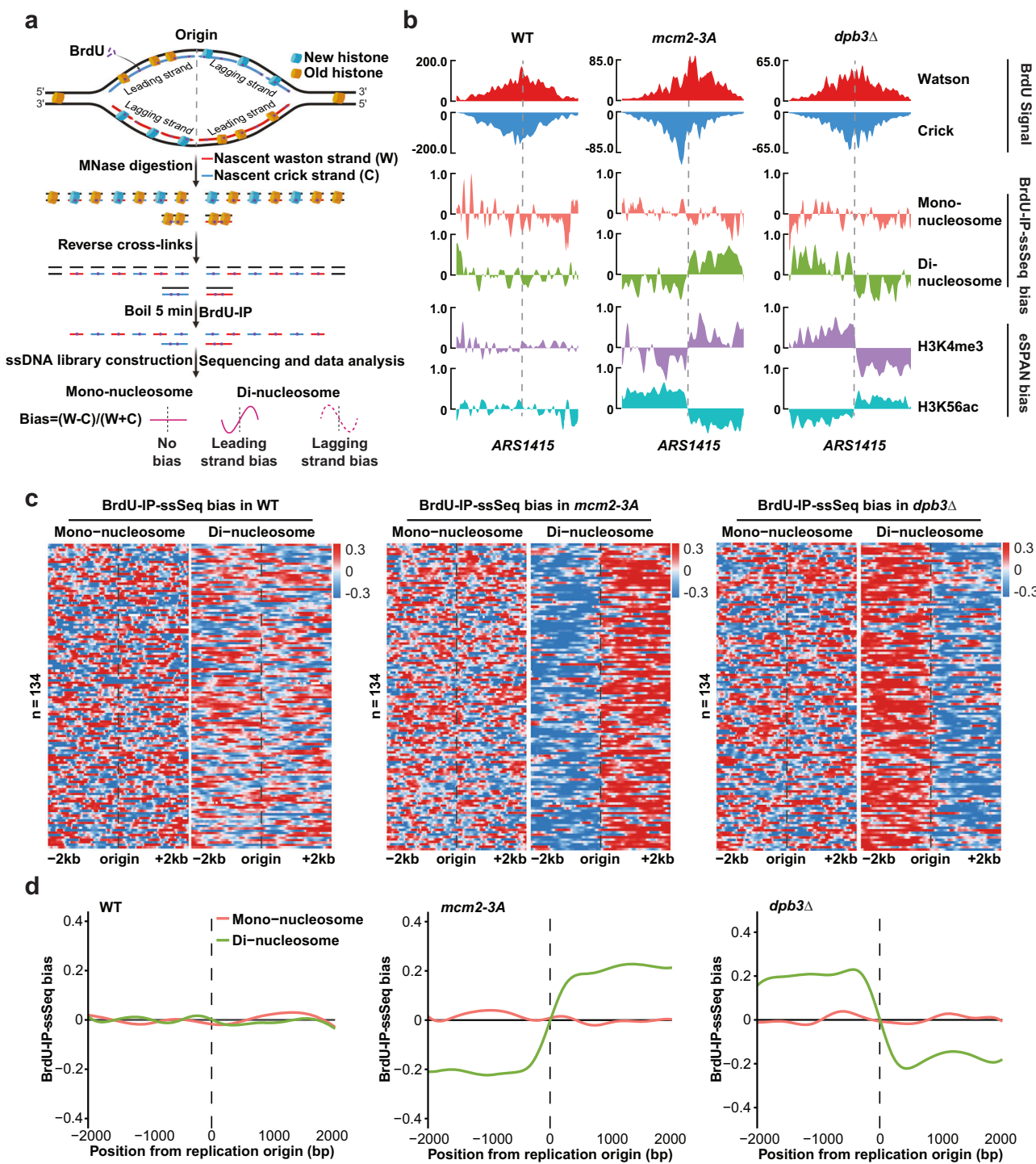


**Fig. 1 | More di-nucleosomes are detected at leading than lagging strands in *mcm2-3A* cells, with an opposite pattern observed in *dpb3Δ* cells.** **a** An outline of the experimental strategy for the BrdU-IP-ssSeq method with the *mcm2-3A* cells as the example. Yeast cells released from G1 arrest were pulsed with BrdU. Following MNase digestion, newly synthesized DNA was immunoprecipitated using antibodies against BrdU followed by strand-specific (ss) sequencing. The sequenced reads were mapped to both Watson strand (W, red) and Crick strand (C, blue) of the reference genome. Sequence reads with the fragment size of a mono-nucleosome (120–200 bp) and a di-nucleosome (250–400 bp) were separated and used to calculate the relative abundance of mono-nucleosome or di-nucleosome at leading and lagging strands using the formula:  $(W - C)/(W + C)$ , which is called BrdU-IP-

ssSeq bias. **b** A snapshot of the BrdU-IP-ssSeq signals, calculated BrdU-IP-ssSeq bias of mono-nucleosomes and di-nucleosomes as well as H3K4me3 and H3K56ac eSPAN bias at *ARS1415* in *WT*, *mcm2-3A*, and *dpb3Δ* cells. The dashed line indicates the origin locus. **c** Heatmaps depicting the BrdU-IP-ssSeq bias for mono-nucleosomes and di-nucleosomes in *WT*, *mcm2-3A*, and *dpb3Δ* cells surrounding each of the 134 early-firing replication origins, ranked from top to bottom based on replication efficiency. **d** Average BrdU-IP-ssSeq bias of mono-nucleosomes and di-nucleosomes in *WT*, *mcm2-3A*, and *dpb3Δ* cells surrounding 134 early-firing replication origins (−2000 bp to 2000 bp). Schematic in **a** was created in BioRender. Zhou, H. (2024) <https://BioRender.com/n10i983>.

strands in *mcm2-3A* cells. In contrast, more di-nucleosomes were formed at lagging strands than leading strands in *dpb3Δ* mutant cells.

Tetra-nucleosomes are considered a fundamental unit of chromatin fibers and are proposed to play a crucial role in the chromatin landscape<sup>53</sup>. Tetra-nucleosome-sized fragments ( $600 \pm 100$  bp) were few in each independent repeat because of MNase digestion and/or library preparation (large fragments were removed). We, therefore, combined sequence reads of tetra-nucleosome-sized fragments of all repeats in each sample and calculated their relative abundance at leading and lagging strands in *mcm2-3A* and *dpb3Δ* cells (Supplementary Fig. 2a, b). Consistent with the patterns observed for di-nucleosome-sized fragments (Fig. 1), we observed that more tetra-nucleosomes were formed leading strand than lagging strands in *mcm2-3A* cells, whereas more tetra-nucleosomes were formed at lagging strands than leading strands in *dpb3Δ* mutant cells. We noticed that the difference in tetra-nucleosome sized fragments between leading and lagging strands in *mcm2-3A* and *dpb3Δ* cells was about 2-fold larger than the corresponding difference in di-nucleosome-sized fragments. Together, these results indicate that nucleosome organization in nascent chromatin in *mcm2-3A* and *dpb3Δ* cells are disorganized differentially at leading and lagging strands.

### The average nucleosome repeat length (NRL) at leading strand is different from that at lagging strands in *mcm2-3A* and *dpb3Δ* mutant cells

The generation of different amounts of di-nucleosomes and tetra-nucleosomes at leading and lagging strands in *mcm2-3A* and *dpb3Δ* cells are likely due to the presence of irregular nucleosome arrays in nascent chromatin where closely-packed di-nucleosomes/tetra-nucleosomes are inaccessible to MNase digestion, leading to a high probability of generating these fragments (Supplementary Fig. 1i). To test this idea, we calculated nucleosome repeat length (NRL) of the leading and lagging strands in wild type, *mcm2-3A*, and *dpb3Δ* mutant cells. NRL, which encompasses both the nucleosome size and linker DNA length, denotes the average distance between the centers of neighboring nucleosomes. As controls, we also analyzed the NRL of each input sample before BrdU immunoprecipitation. No significant differences in the NRL were detected among input samples of wild type, *mcm2-3A*, and *dpb3Δ*, with the average NRL close to 161 bp (Supplementary Fig. 3a, b). In wild type cells, NRLs of the leading and lagging strands were similar, with the average NRLs of 170 bp (Fig. 2a, d), consistent with the idea that nucleosome occupancy and position at leading and lagging strands were similar. In *mcm2-3A* mutant cells, NRL at the lagging strand was about 188 bp and significant longer than leading strands (164 bp) (Fig. 2b, d). In contrast, NRL of leading strands in *dpb3Δ* cells exceeded those of lagging strands (Fig. 2c, d). The increase in NRL of lagging strands in *mcm2-3A* cells and leading strands in *dpb3Δ* cells was likely due to preferential enrichment of H3K56ac at lagging strands in *mcm2-3A* and leading strands in *dpb3Δ* cells<sup>13,14</sup> (see results below). These results support the idea that an extended NRL facilitates greater MNase accessibility, consequently reduces amount of di-nucleosomes/tetra-nucleosomes on the lagging strand in *mcm2-3A* cells and leading strands in *dpb3Δ* cells. These results indicate that the enrichment of di-nucleosome- and tetra-nucleosome-sized fragments at leading and lagging strands in *mcm2-3A* and *dpb3Δ* cells, respectively, likely arises from the closely-packed nucleosomes in nascent chromatin.

To test this idea further, we synchronized wild type and *mcm2-3A* cells in G1 phase using α-factor and then released these cells into S phase in the presence of the nucleotide analog BrdU for 30 min to label nascent chromatin. To block further BrdU incorporation at latter time points, we added thymidine to each culture 30 minutes after release. We then harvested cells at 30, 60, and 90 minutes after the release from G1 block (Fig. 2e), which corresponds to early S phase, late S phase, and G2 phase of the cell cycle<sup>54</sup>, and analyzed di-nucleosomes

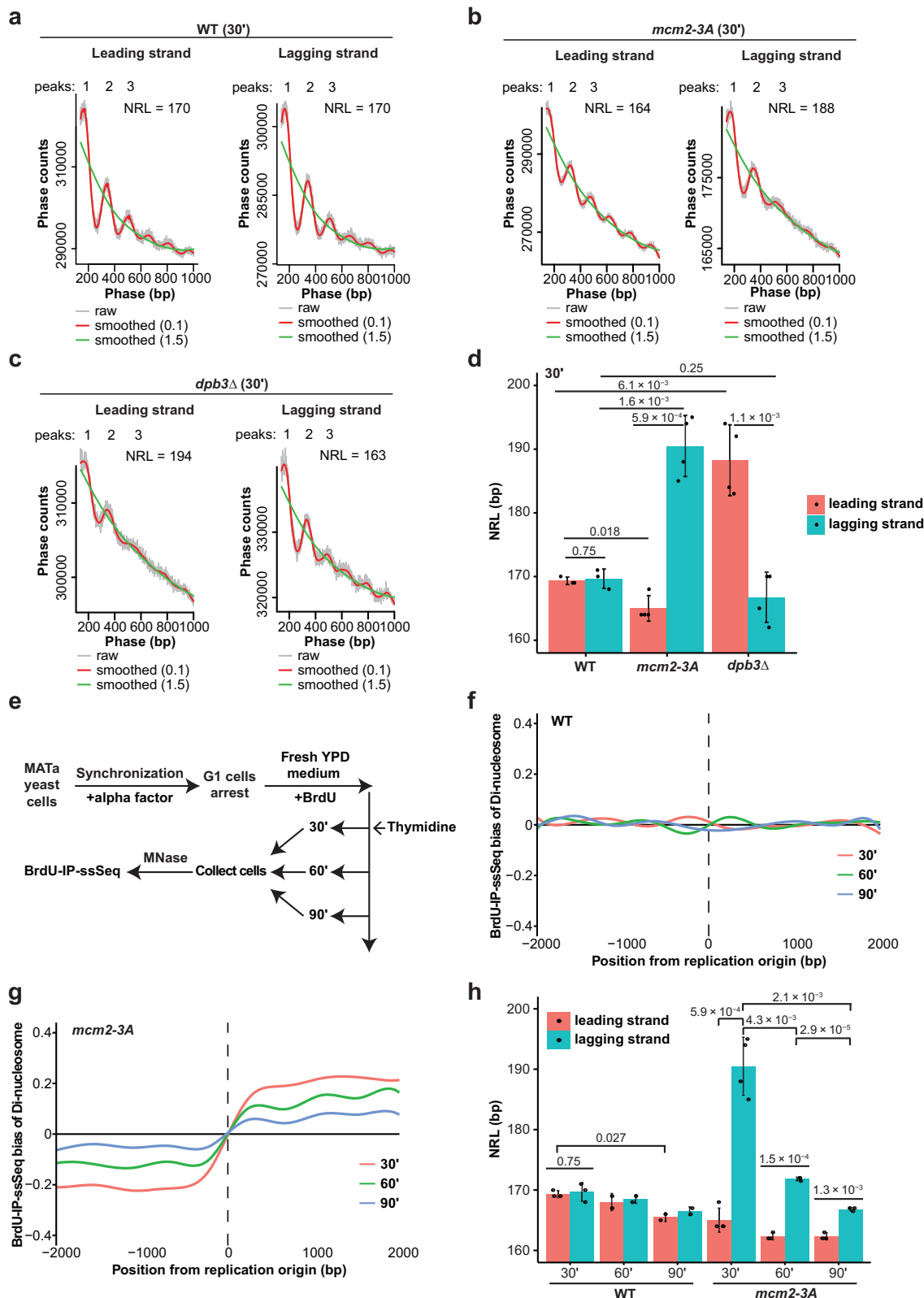
and nucleosome repeat length at the same chromatin regions marked by BrdU. In both wild type and *mcm2-3A* cells, an equal amount of mono-nucleosomes was detected at leading and lagging strands at these three time points (Supplementary Fig. 3c, d). In contrast, while di-nucleosomes detected at leading and lagging strands were also similar in wild type cells (Fig. 2f), the enrichment of di-nucleosomes at leading strands in *mcm2-3A* cells gradually decreased from early S phase to G2 phase of the cell cycle (Fig. 2g). The NRL of both leading and lagging strands in both WT and *mcm2-3A* cells showed a gradual decline trend over the time course of the experiments (Fig. 2h and Supplementary Fig. 3e-h), with a marked reduction of NRL at lagging strands in *mcm2-3A* cells. Furthermore, the disparity in NRL between leading and lagging strands in *mcm2-3A* cells was remarkably diminished during the time course. These results show that more closely packed nucleosomes including di-nucleosomes are formed soon after DNA replication during early S phase and these closely-packed nucleosomes are resolved at late S or G2/M phase of the cell cycle. These results also indicate that chromatin maturation alleviates the NRL differences between leading and lagging strands in *mcm2-3A* cells.

### H3K56ac and H3K4me3 are associated with the formation of di-nucleosomes in *mcm2-3A* and *dpb3Δ* cells

To understand how closely-packed nucleosomes including more-closely packed di-nucleosomes are formed in *mcm2-3A* and *dpb3Δ* cells, we first analyzed chromatin features associated with di-nucleosomes formed at nascent chromatin in wild type, *mcm2-3A*, and *dpb3Δ* cells. Briefly, we calculated the relationship between di-nucleosomes of nascent chromatin in WT, *mcm2-3A*, and *dpb3Δ* cells and each of the 25 histone modifications and the histone variant H2A.Z in wild type cells<sup>55</sup>, and constructed heatmaps for each modification across quintiles of di-nucleosome occupancy derived from both leading and lagging strands (Supplementary Fig. 4a). We found that nascent chromatin regions with lowest di-nucleosome signals (first quintile) were enriched for H2A.Z and histone acetylation marks linked to open chromatin. In contrast, nascent chromatin regions with the highest di-nucleosome occupancy are associated with histone methylation and H4K16 acetylation, a mark linked to chromatin condensation and inhibition of the ISWI chromatin remodeler<sup>56</sup>. Because of differences in di-nucleosomes at leading and lagging strands in *mcm2-3A* and *dpb3Δ* cells, we calculated the delta Z-scores between leading and lagging strands in individual samples to investigate histone modifications associated with changes in di-nucleosome patterns between leading and lagging strands (Supplementary Fig. 4b). In wild type cells, there were little changes between leading and lagging strands. In contrast, H3K56ac and H3K4me3, two marks that are asymmetrically distributed at leading and lagging strands, appear to be the top candidates associated with changes in di-nucleosome distribution in *mcm2-3A* and *dpb3Δ* cells (Supplementary Fig. 4b).

### Asymmetric distribution of H3K4me3 is unlikely a cause for the formation of closely packed di-nucleosomes in *mcm2-3A* cells

To determine the potential influence of H3K4me3, a marker indicative of parental nucleosomes that are enriched at leading strands in *mcm2-3A* cells, we asked whether the enrichment of di-nucleosomes at leading strands in *mcm2-3A* cells was changed upon depletion of Swd1, a COMPASS complex subunit essential for H3K4 methylation<sup>57</sup>, using an auxin-inducible degron (Swd1-AID). Specifically, we degraded Swd1 with the addition of IAA (Supplementary Fig. 5a). Subsequently, we released these G1 phase cells with/without Swd1 degradation into S phase, and collected samples at different time points for analysis of nucleosomes in nascent chromatin by BrdU-IP-ssSeq and the distribution of H3K4me3 at replicating chromatin by eSPAN (Supplementary Fig. 5a). As reported previously<sup>54</sup>, the enrichment of H3K4me3 at leading compared to lagging strands remained unchanged over time course in the presence of IAA, whereas it reduced over time in the



absence of IAA due to methylation of H3K4 on newly synthesized H3 by COMPASS complex (Supplementary Fig. 5b, c). We observed little BrdU-IP-ssSeq bias of mono-nucleosomes regardless of the presence or absence of IAA (Supplementary Fig. 5d, e). Conversely, the BrdU-IP-ssSeq bias of di-nucleosomes at replicated chromatin diminished over time in both IAA-treated and untreated cells (Supplementary Fig. 5f, g). These results indicate that the asymmetric distribution of H3K4me3 at

leading strands is unlikely causally linked to the enrichment of di-nucleosomes at leading strands in *mcm2-3A* cells.

### H3K56ac regulates nucleosome repeat length and closely-packed di-nucleosomes in *mcm2-3A* cells

Next, we asked whether H3K56ac plays any role in governing di-nucleosome asymmetry in *mcm2-3A* cells. To do this, we analyzed the

**Fig. 2 | Nucleosome repeat length (NRL) at leading strands is different from that of lagging strands in *mcm2-3A* and *dpb3A* cells.** **a–c** Phasograms of the NRL of nascent chromatin in WT (a), *mcm2-3A* (b), and *dpb3A* cells (c). Phasogram, which illustrates phase frequencies, is utilized to unveil the presence of consistently spaced nucleosome arrays. The NRL is estimated from the frequencies of alignment distances on the same strand (phasogram) by calculating the slope of a linear fit to the modes in the phasogram. Phasograms (Red line, span = 0.1, and green line, span = 1.5) were derived from BrdU-IP-ssSeq signals of a representative raw data (gray line). **d** Bar plots quantification of the NRL of leading and lagging strands using BrdU-IP-ssSeq datasets from 3 independent repeats in wild type (N = 3), 4

independent repeats in both *mcm2-3A* and *dpb3A* cells (N = 4). **e** An outline of experimental procedures to monitor nucleosome repeat length at replicated regions during cell cycle progression. **f, g** Average BrdU-IP-ssSeq bias of di-nucleosomes in WT (f) and *mcm2-3A* cells during cell cycle progression (g). **h** Bar plot quantification of the NRL of leading and lagging strands in WT and *mcm2-3A* cells. Please note that there are 4 repeats for 30 min time points and 2 repeats at 60 and 90 min time points. **d** and **h**, two-sided Student's t-test was performed. Data were presented as mean values  $\pm$  standard deviation; error bars represent standard deviation. Source data are provided as a Source Data file.

effect of deletion of Rtt109, the H3K56 acetyltransferase, on the formation of closely-packed di-nucleosomes in *mcm2-3A* cells. The BrdU-IP-ssSeq bias of di-nucleosomes in *rtt109Δ* was similar to that of WT, suggesting that an equal amount of di-nucleosomes were formed at leading and lagging strands in *rtt109Δ* cells. Remarkably, *RTT109* deletion notably diminished the enrichment of di-nucleosomes at leading strand in *mcm2-3A* cells based on analysis of individual origins (Fig. 3a), and the average BrdU-IP-ssSeq bias of di-nucleosomes of all early firing origins (Fig. 3b). In contrast, loss of Rtt109 had no apparent effects on the H3K4me3 eSPAN bias in *mcm2-3A* cells (Fig. 3c). These results show that deleting Rtt109 does not affect the parental histone transfer in *mcm2-3A* cells. Furthermore, these results provide additional support to the idea that H3K4me3 does not play a causal role in the formation of closely packed di-nucleosomes in *mcm2-3A* cells. Instead, Rtt109 and potentially H3K56ac are important for this process.

In addition to H3K56, Rtt109 also acetylates lysine residues at the H3 N-terminus including H3K27<sup>22</sup>. We, therefore generated the *mcm2-3A H3K56R* double mutant strain and performed the BrdU-IP-ssSeq and H3K4me3 eSPAN analysis. Similar to *RTT109* deletion, the BrdU-IP-ssSeq bias of di-nucleosomes was markedly reduced *mcm2-3A H3K56R* cells compared to *mcm2-3A* cells (Fig. 3d). Furthermore, mutations of *RTT109* and *H3K56R* markedly reduced the NRL of lagging strands in *mcm2-3A* cells (Fig. 3e). Finally, the levels of di-nucleosomes were markedly reduced at the leading strand and increased at the lagging strand upon mutating either *RTT109* or *H3K56* in *mcm2-3A* cells (Fig. 3f). In contrast, the H3K56R mutation had no apparent effects on H3K4me3 eSPAN bias in *mcm2-3A* cells (Fig. 3g). These results indicate that H3K56ac plays a crucial role in preventing the formation of closely-packed nucleosomes in nascent chromatin, and that H3K27ac likely has little impact on this process.

### Effects of *ISWI* and *CHD1* deletion on the formation of closely-packed nucleosomes in nascent chromatin

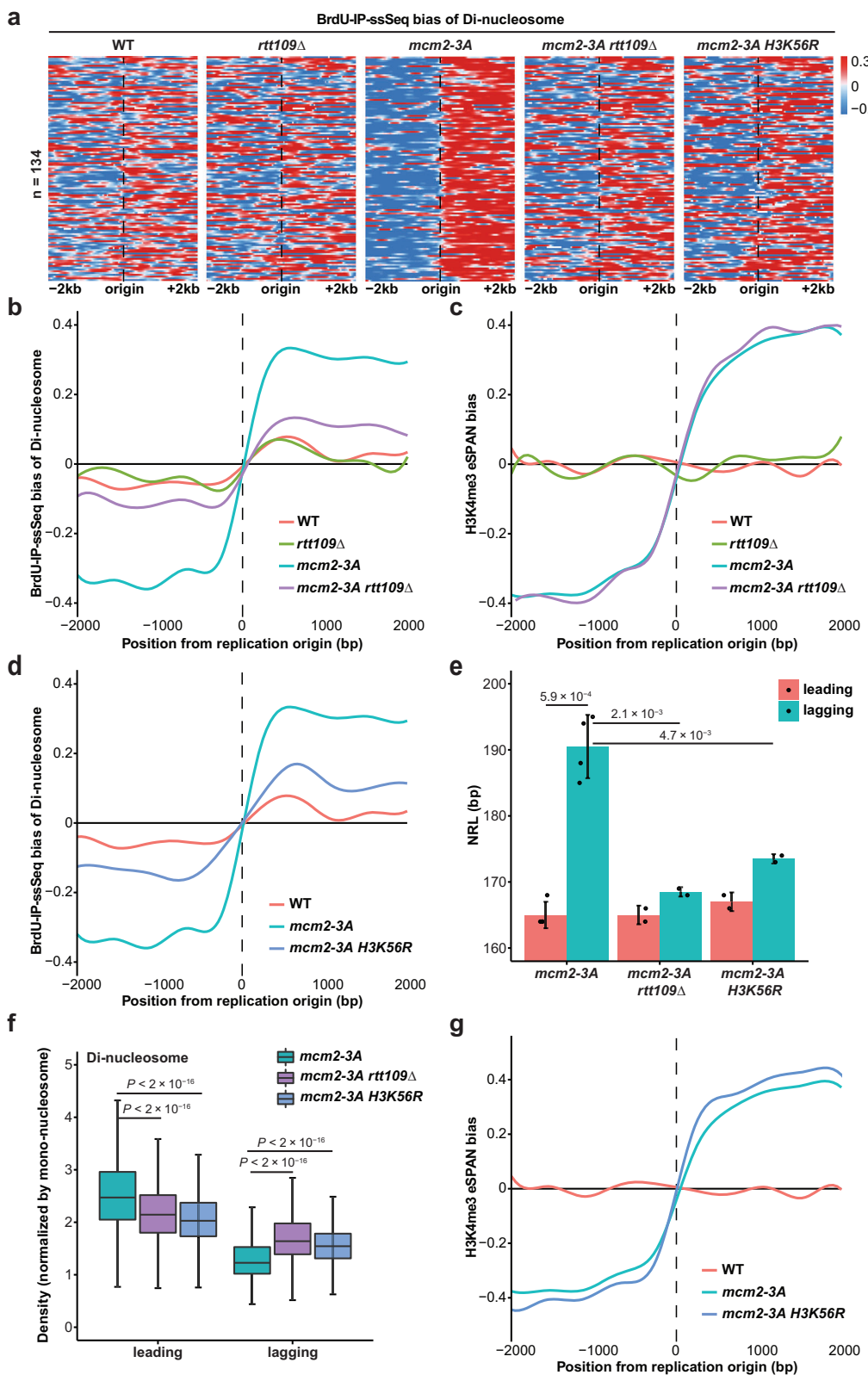
In cells lacking chromatin remodelers *ISWI* and *Chd1*, closely packed di-nucleosomes are formed near transcription start sites<sup>48,58</sup>. Furthermore, chromatin remodelers, including *Isw1* and *Chd1*, work with origin recognition complex (ORC) to facilitate the establishment of a phased nucleosome array at replication origins<sup>59</sup>. We therefore asked whether *Isw1* and *Chd1* are involved in remodeling closely-packed nucleosomes in *mcm2-3A* cells. Deletion of *ISWI* or *CHD1* had no apparent effects on the relative amount of mono-nucleosomes at leading and lagging strands in *mcm2-3A* mutant cells (Supplementary Fig. 6a). However, the enrichment of di-nucleosomes at leading strands was substantially reduced in *mcm2-3A isw1Δ* double mutant cells compared to *mcm2-3A* cells (Fig. 4a and Supplementary Fig. 6b). There were no detectable differences in the eSPAN bias for H3K4me3 and H3K56ac between *mcm2-3A* and *mcm2-3A isw1Δ* double mutant cells (Fig. 4b, c), suggesting that *ISWI* deletion, while affecting closely-packed nucleosomes at leading and lagging strands, did not affect parental histone transfer in *mcm2-3A* mutant cells. Deletion of *CHD1* also reduced BrdU-IP-ssSeq bias for di-nucleosomes, but to a lesser magnitude compared with *ISWI* deletion (Fig. 4d–f). These results indicate that *Isw1* is a dominant chromatin remodeler to resolve close-

packed nucleosomes in nascent chromatin compared to *Chd1*. Furthermore, the NRL of the lagging strand was shorter in *isw1Δ mcm2-3A* or *chd1Δ mcm2-3A* double mutant cells compared to the *mcm2-3A* mutant (Fig. 4g). Relatively to mono-nucleosomes in each strain, deletion of *CHD1* and *ISWI* in *mcm2-3A* cells resulted in reduced di-nucleosome levels at leading strand and an increased di-nucleosome levels at lagging strands (Fig. 4h), an effect similar to that of mutating *RTT109* or H3K56. Finally, we found that the *mcm2-3A chd1Δ rtt109Δ* triple mutant cells exhibited similar distribution of di-nucleosomes at leading and lagging strands to those observed in the *mcm2-3A rtt109Δ* double mutant cells. Furthermore, NRL at leading and lagging strands were also comparable between the triple and double mutant cells (Supplementary Fig. 6c–e). These results indicate that chromatin remodelers *Isw1* and *Chd1* work with H3K56 acetylation, likely functioning downstream of H3K56ac, to resolve closely-packed nucleosomes in nascent chromatin.

### H3K56ac enhances the chromatin remodeling activity of *Isw1a*, *Isw1b* and *SNF2h*

Previously, H3K56ac was found to have modest effects on remodeling activity of RSC and SWI/SNF, enhancing activity of SWI/SNF and RSC by 1.2–1.4-fold<sup>60</sup>. Because *Isw1* and *Chd1* likely function in the same pathway to resolve closely-packed nucleosomes in *mcm2-3A* cells, we investigated whether H3K56ac influences the chromatin remodeling activity by *Isw1* in vitro. *Isw1* is the catalytic subunit of two chromatin remodelers in budding yeast, *Isw1a* (consisting of *Isw1* and *loc3*) and *Isw1b* (consisting of *Isw1*, *loc2*, and *loc4*)<sup>61</sup>. We first tested the activity of *Isw1a* and *Isw1b* complexes, purified from yeast cells, on Widom 601 mono-nucleosomes formed with histone octamer with or without H3K56ac (Supplementary Fig. 7a–c). Consistent with prior work<sup>62</sup>, *Isw1a* shifted end-positioned 80N0 nucleosomes toward central positions on DNA (Fig. 5a). Nucleosome sliding by *Isw1a* was approximately 2.7-fold faster on H3K56ac-nucleosomes compared with unmodified nucleosomes (Fig. 5b, c). *Isw1b* shifted centered 40N40 nucleosomes toward DNA ends, and we found that the *Isw1b* sliding rate was 2.1-fold faster on H3K56ac-nucleosomes compared to unmodified nucleosomes (Fig. 5c, d and Supplementary Fig. 7d). Thus, both *ISWI* complexes show a marked higher activity for H3K56ac-containing nucleosomes compared to unmodified ones.

Human *ISWI* family chromatin remodelers contains seven members, *SNF2h*, *ACF*, *CHRAC*, *WICH*, *NoRC*, *RSF*, and *NURF*<sup>41,63</sup>. Using a high-throughput in vitro nucleosome remodeling assay, it has been shown that histone modifications impact the activity of these different chromatin remodelers<sup>64</sup>. We reanalyzed the effects of H3K4me3, H2A.Z and acetylation of 21 different histone lysine residues on the activities of these 7 *ISWI* remodelers and *CHD4*. Consistent with published results, all these chromatin remodelers showed a higher activity towards H2A.Z-containing nucleosomes compared to H3K4me3-containing or acetylated H4-containing nucleosomes. Notably, we found that H2A.Z was enriched at regions with lowest closely-packed di-nucleosomes in nascent chromatin (Supplementary Fig. 4a). Importantly, we found that human *ISWI* and *CHD4* remodelers exhibited a marked higher activity towards H3K56ac-modified nucleosomes than H3K4me3-modified nucleosomes, with the effects



of H3K56ac on each ISWI family member more pronounced than CHD4 (Fig. 5e). We therefore tested the effects of H3K56ac on the activity of human SNF2h in vitro, and found that it exhibited a markedly higher activity towards H3K56ac-modified nucleosomes than unmodified ones (Fig. 5f, g and Supplementary Fig. 7e). Taken together, these findings indicate that H3K56ac can augment chromatin remodeling activity of both yeast and human ISWI family chromatin remodelers.

#### Persistent H3K56ac outside S phase prevents chromatin maturation, resulting in genome instability

In budding yeast, Hst3 and Hst4 are primarily responsible for the deacetylation of histone H3 lysine 56, which happens at G2/M phase of the cell cycle, and in their absence, over 90% of H3 proteins are acetylated at K56<sup>35</sup>. Therefore, we determined impact of deletion of Hst3 and Hst4 in *mcm2-3A* cells in the formation of closely-packed

**Fig. 3 | H3K56ac regulates closely-packed nucleosomes and nucleosome repeat length of nascent chromatin.** **a** Heatmap depicting the BrdU-IP-ssSeq bias of di-nucleosomes in strains with genome type indicated at top surrounding each of the 134 early DNA replication origins (-2000 to +2000), sorted on the basis of replication efficiency. **b** and **d** Average BrdU-IP-ssSeq bias of di-nucleosomes within 4 kb of 134 early-firing replication origins in wild type, *rtt109Δ*, *mcm2-3A*, *mcm2-3A rtt109Δ* (**b**) and *mcm2-3A H3K56R* (**d**) cells. **c** Average bias of H3K4me3 eSPAN bias within 4 kb of 134 early-firing replication origins in yeast strains with relevant genome type indicated. **e** Bar plot quantification of the NRL at nascent leading and lagging strands in *mcm2-3A* (N = 4 independent experiments), *mcm2-3A rtt109*

(N = 2 independent experiments), and *mcm2-3A H3K56R* (N = 2 independent experiments) mutant cells. P values were calculated with two-sided Student's t-test was performed. Data were presented as mean values  $\pm$  standard deviation; error bars represent standard deviation. **f** Box plots of di-nucleosome density at the early replicated genes shared by three strains (replicated genes = 1319). Density is normalized by mono-nucleosome levels in each strain. Box plots show the median, 25% and 75% quartiles and minimal and maximal values. P values were calculated using two-sided Mann-Whitney-Wilcoxon tests. **g** Average bias of H3K4me3 eSPAN bias within 4 kb of 134 early-firing replication origins in wild type, *mcm2-3A*, and *mcm2-3A H3K56R* cells. For **e** and **f**, source data are provided as a Source Data file.

nucleosomes in nascent chromatin using BrdU-IP-ssSeq. We also monitored the distribution of H3K56ac and H3K4me3 at replicating DNA strands using eSPAN in *mcm2-3A hst3Δ hst4Δ* cells. Because H3K56ac cannot be erased during G2/M phases, H3K56ac in *hst3Δ hst4Δ* mutant cells will be found on all new H3-H4 and 80-90% of parental H3-H4 (Fig. 6a). Consequently, the H3K56ac eSPAN bias toward lagging strands was eliminated in *mcm2-3A hst3Δ hst4Δ* triple mutant cells compared to *mcm2-3A* cells (Fig. 6b). In contrast, deletion of *HST3* and *HST4* in *mcm2-3A* cells did not affect H3K4me3 eSPAN bias (Fig. 6c), suggesting that deletion of *HST3* and *HST4* does not affect parental histone transfer. Interestingly, we observed a slight decrease in the BrdU-IP-ssSeq bias of di-nucleosomes in *mcm2-3A hst3Δ hst4Δ* mutant cells compared to *mcm2-3A* cells (Fig. 6d and Supplementary Fig. 8a), while having little impact on the relative amount of mono-nucleosomes at leading and lagging strands (Supplementary Fig. 8b). Importantly, compared to *mcm2-3A* cells, a longer NRL and reduced di-nucleosome signals at both leading and lagging strands were detected in *mcm2-3A hst3Δ hst4Δ* triple mutant cells (Fig. 6e, f). Similarly, a slightly extended NRL was observed at both the leading and lagging strands of *hst3Δ hst4Δ* double mutant cells compared to WT cells (Fig. 6e). These results indicate that the persistent presence of H3K56ac in *hst3Δ hst4Δ* cells likely prevents chromatin maturation, likely due to continuous and excessive chromatin remodeling.

Cells lacking *HST3* and *HST4* are sensitive to DNA damage agents. We, therefore, asked whether the DNA damage sensitivity is due to their impact on chromatin maturation. As reported<sup>26</sup>, yeast cells lacking *Hst3* and *Hst4* are sensitive to hydroxyurea and CPT. Cells with a deletion of either *CHD1* or *ISW1* in an otherwise wild type background were relatively insensitive to these treatments with HU and CPT (Fig. 6g). In contrast, deleting *CHD1* or *ISW1* in *hst3Δ hst4Δ* cells partially suppressed HU and CPT sensitivity of *hst3Δ hst4Δ* (Fig. 6g). These results support the idea that the persistent presence of H3K56ac inhibits chromatin maturation and causes genome instability.

## Discussion

Chromatin is essential for maintaining gene transcriptional programs and cellular identity, both through inhibiting easy access to DNA and providing a physical substrate for epigenetic memory. With the dramatic disassembly coupled to passage of replication forks, chromatin must be faithfully reassembled in the wake of DNA replication. It has been well documented that chromatin structure immediately after DNA replication is much less well organized than in steady state. Previous studies have documented the potential roles of gene transcription and ATP-dependent chromatin remodelers in remodeling nascent and disorganized chromatin into their steady state<sup>36-38</sup>. Here, we show that H3K56ac, a mark on newly synthesized histones, aids remodeling of closely packed nucleosomes in nascent chromatin (Fig. 7a, b). In vitro, H3K56ac enhances the activity of ISW1 chromatin remodelers and its human counterpart, SNF2h. Furthermore, we found that the persistent presence of H3K56ac in cells lacking *Hst3* and *Hst4*, two H3K56ac de-acetylases, inhibits chromatin maturation, which may contribute to genome instability. These studies reveal a previously unknown role of H3K56ac and an undocumented mechanism in chromatin maturation.

## The formation of closely packed nucleosomes in nascent chromatin following DNA replication

Nascent chromatin immediately after DNA replication is more susceptible to digestion by nucleases compared to steady state mature chromatin, indicating that nucleosomes in nascent chromatin are irregularly spaced<sup>36</sup>. We found that the presence of closely packed nucleosomes including di-nucleosome-sized and tetra-nucleosome-sized fragments is a feature in nascent chromatin. In wild type cells, parental and newly synthesized H3-H4 tetramers are equally distributed at leading and lagging strands of DNA replication forks<sup>13</sup>. Furthermore, equal amounts of di-nucleosomes were released by MNase digestion from nascent leading and lagging strands. Therefore, it has been challenging to discern whether di-nucleosomes generated by MNase digestion are due to incomplete digestion by MNase or a feature in nascent chromatin. In *mcm2-3A* cells defective in parental histone transfer to lagging strands, parental histone H3-H4 (marked by H3K4me3) and newly synthesized H3-H4 (marked by H3K56ac) are enriched at leading strands and lagging strands, respectively. In this setting, we surprisingly observed that more di- and tetra-nucleosomes were detected at leading strands compared to lagging strands. In contrast, in *dpb3Δ* cells defective in parental histone transfer to leading strands, more di- and tetra-nucleosomes were generated from lagging strands than leading strands. Furthermore, we found that nucleosome repeat length at leading strands in *mcm2-3A* mutant cells is markedly shorter than that of lagging strands, while nucleosome repeat length in *dpb3Δ* cells showed an opposite pattern. These results indicate that the differential amount of di- and tetra-nucleosomes at leading and lagging strands in *mcm2-3A* or *dpb3Δ* cells likely reflect closely-packed nucleosomes that are resistant to MNase digestion. In both wild type and *mcm2-3A* cells, regions with low di-nucleosomes abundance in nascent chromatin are associated with H2A.Z. Previously, it was shown that mammalian ISWI family chromatin remodelers show a markedly higher activity towards H2A.Z-nucleosomes<sup>64</sup>. Therefore, the formation of closely-packed nucleosomes in nascent chromatin likely also occur in wild type cells. Remodeling of these closely-packed nucleosomes likely represent a key event in chromatin maturation following DNA replication. Recently, it has been shown that during gene transcription, hexosome is formed directly adjacent to a nucleosome, and these hexosome-nucleosome intermediates can be resolved by the chromatin remodeler Chd1<sup>65</sup>. Therefore, it is possible closely-packed nucleosomes detected in nascent chromatin contain these overlapping hexosome-nucleosome particles or related overlapping di-nucleosomes. Future studies are needed to resolve the precise structural information of closely-packed nucleosome in nascent chromatin. Finally, because Mcm2 and Dpb3-Dpb4 (POLE3-POLE4 in mammalian cells) are also involved in parental histone transfer in mammalian cells<sup>13-15,66</sup>, it would be interesting to determine whether closely-packed nucleosomes are also asymmetrically distributed at leading and lagging strands in Mcm2, POLE3, and POLE4 mutant cells defective in parental histone transfer.

## H3K56ac promotes chromatin remodeling

It is generally accepted that chromatin remodelers facilitate the maturation of nascent chromatin following DNA replication in vitro

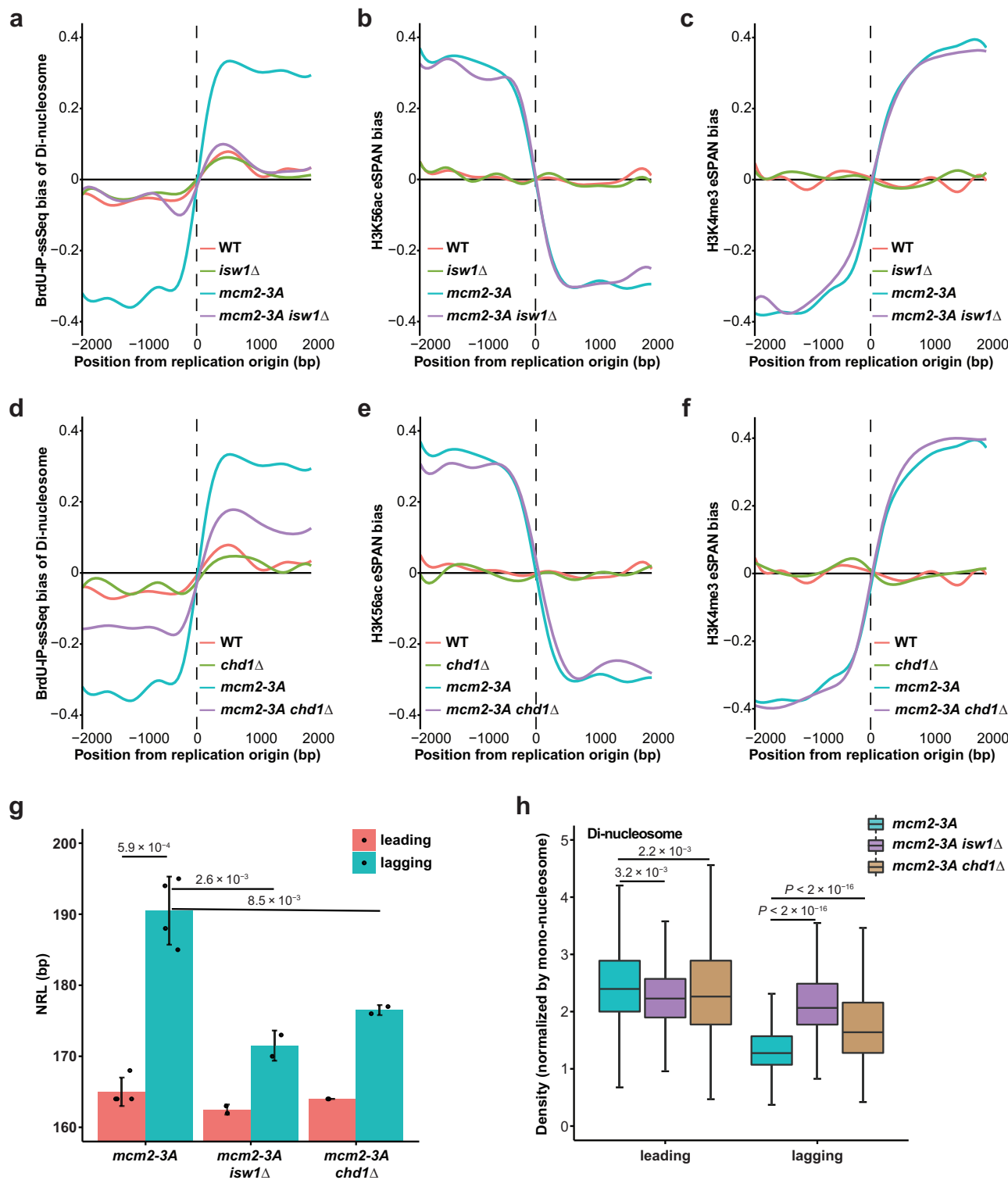
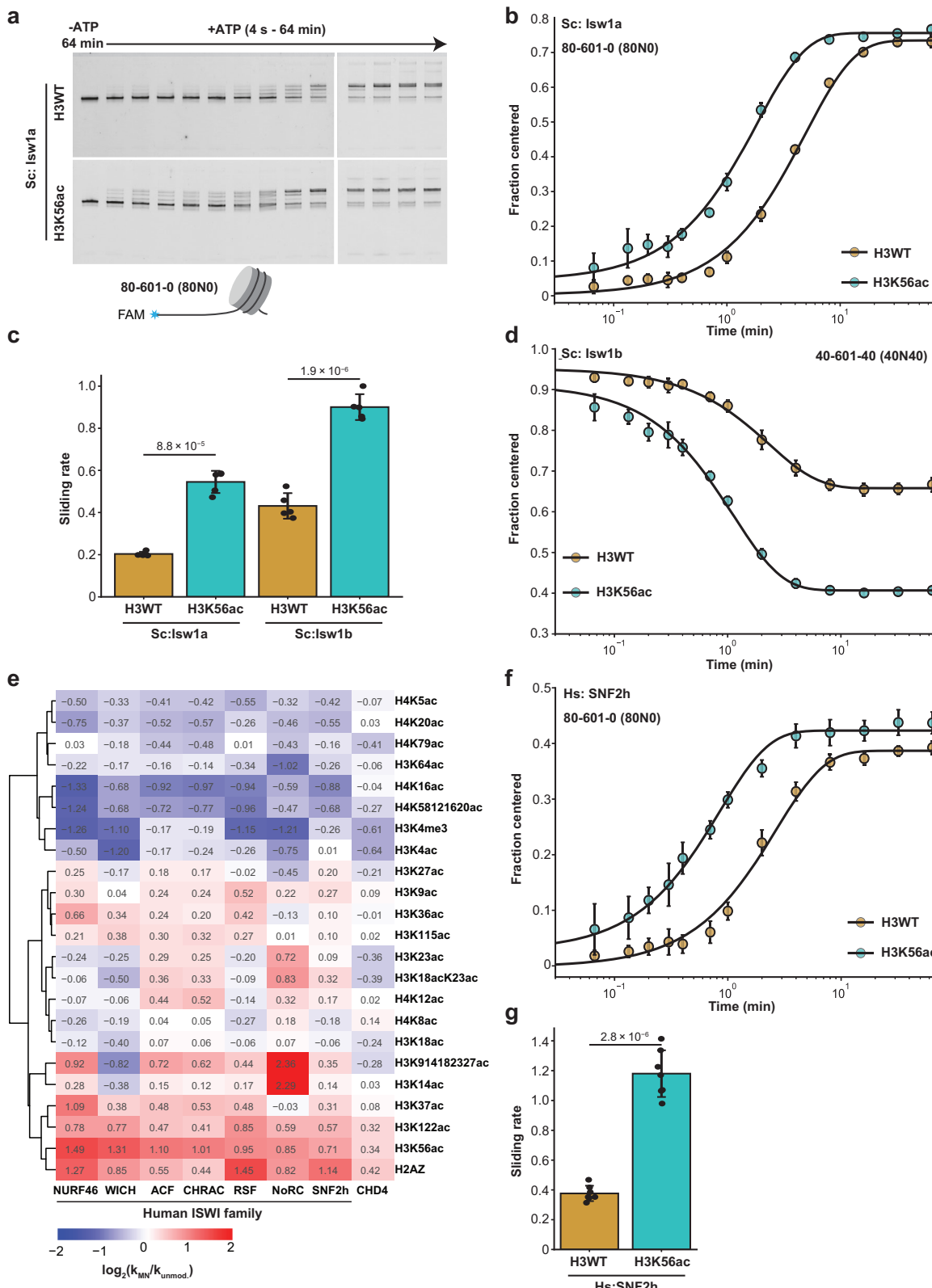


**Fig. 4 | Chromatin remodelers Isw1 and Chd1 modulate the asymmetric enrichment of di-nucleosomes at leading strands in *mcm2-3A* cells. a and d** Average BrdU-IP-ssSeq bias of di-nucleosomes within 4 kb of 134 early-firing replication origins in yeast strains with relevant genome type identified. **b and e** Effects of *CHD1* and *ISW1* deletion on the average H3K56ac eSPAN bias. **c and f** Effects of *CHD1* and *ISW1* deletion on H3K4me3 eSPAN bias. **g** Bar plot quantification of the NRL at leading and lagging strands in *mcm2-3A* ( $N=4$  independent experiments), *mcm2-3A isw1Δ* ( $N=2$  independent experiments), *mcm2-3A chd1Δ*

cells ( $N=2$  independent experiments). P values were calculated with two-sided Student's t-test. Data were presented as mean values  $\pm$  standard deviation; error bars represent standard deviation. **h** Box plots of di-nucleosome density across the early replicated genes shared by three strains (replicated genes = 1278). Density is normalized by mono-nucleosome levels in each strain. Box plots show the median, 25% and 75% quartiles and minimal and maximal values. P values were calculated using two-sided Mann-Whitney-Wilcoxon tests. For **g** and **h**, source data are provided as a Source Data file.



and in cells. Furthermore, previous studies indicate that nascent chromatin at different loci, marked by different histone modifications, return to their steady states at different kinetics. However, it was largely unexplored whether histone modifications in nascent chromatin, which include modifications on parental histones and newly synthesized histones, play a direct role in nascent chromatin maturation. Here we show that H3K56ac plays an important role in resolving

closely packed nucleosomes in nascent chromatin. This finding was made possible by analyzing di-nucleosomes at leading and lagging strand in *mcm2-3A* cells. In *mcm2-3A* cells, which are defective in parental histone transfer to lagging strands, H3K56ac is enriched at lagging strands<sup>18</sup>. Mutating H3K56 or the responsible acetyltransferase, Rtt109, suppresses the strong asymmetry we observed in *mcm2-3A* cells by reducing the nucleosome repeat length and increasing

**Fig. 5 | H3K56ac enhances the nucleosome sliding activity of Isw1 and SNF2h.** **a** Nucleosome sliding activities of yeast Isw1a using mono-nucleosomes assembled with histone octamers with or without H3K56ac. The first lane serves as a size control without ATP treatment. Created in BioRender. Wang, G. (2024) <https://BioRender.com/u94f365>. **b** Quantification of nucleosome sliding reactions. The end-positioned band intensity was normalized to the total band intensity within each lane. Shown are the means plus standard deviations of five replicates. Lines show the best single exponential fits. **c** Bar plot indicating nucleosome sliding rates of Isw1a and Isw1b on nucleosomes with or without H3K56ac ( $N = 5$  independent experiments, mean  $\pm$  SD). **d** Quantification of nucleosome centering activities of yeast Isw1b on nucleosomes with or without H3K56ac. Shown are the means plus standard deviations of five replicates. Lines show the best single exponential fits.

**e** Heatmap displaying the effects of different histone modifications and H2A.Z on nucleosome sliding activity of human ISWI family chromatin remodelers. Rows were clustered on the basis of chromatin remodeling activity.  $k_{MN}$ , remodeling rate on modified nucleosomes;  $k_{unmod}$ , remodeling rate on unmodified nucleosomes. Values were capped at -4 and 4 for display purposes. **f, g** Effects of H3K56ac on nucleosome sliding activities by human SNF2h ( $N = 7$  independent experiments, mean  $\pm$  SD). Shown are the means plus standard deviations of seven replicates. Lines show the best single exponential fits. P values in (c) and (g) were calculated using two-sided Student's t-test. Data were presented as mean values  $\pm$  standard deviation; error bars represent standard deviation. Source data are provided as a Source Data file.

closely-packed nucleosomes in lagging strands. In contrast, alterations of H3K4me3 levels during S phase do not affect closely packed di-nucleosomes in *mcm2-3A* cells. These results indicate that a deficiency of H3K56ac at leading strands in *mcm2-3A* cells leads to an increase in closely-packed di-nucleosomes.

Mechanistically, we found that H3K56ac increases the chromatin remodeling activity of ISW1 and its human counterpart SNF2h *in vitro*. In cells, while deletion of *ISW1* or *CHD1* suppresses the enrichment of closely packed di-nucleosomes at leading strands in *mcm2-3A* mutant cells, deletion of *ISW1* or *CHD1* did not affect the asymmetric distribution of H3K56ac. These results support the model Isw1 and Chd1 act downstream of chromatin reassembly and may specifically target H3K56ac-nucleosomes to resolve closely-packed di-nucleosomes in nascent chromatin.

How does H3K56ac work with ISW1 family chromatin remodelers and Chd1 in resolving closely-packed di-nucleosomes? H3K56ac is localized at both the entry and exit point of the nucleosome. This modification markedly increases DNA breathing and unwrapping<sup>60</sup>. Isw1a chromatin remodeler, consisting of Isw1 and Ioc3, preferentially binds di-nucleosomes<sup>49</sup>. The cryo-EM structure of Isw1a bound di-nucleosome revealed that DNA binding domain of Isw1 interacts with the entry DNA at the nucleosome edge<sup>67</sup>. *In vitro*, Chd1 chromatin remodeler can sense both entry and exit point of nucleosomes for the generation of regularly spaced nucleosomes<sup>68</sup>. Therefore, it is possible that H3K56ac lowers the binding energy between DNA and histones at the entry and exit point of the nucleosome and thereby enhancing the activity of these chromatin remodelers. Alternatively, H3K56ac, like other modifications, may directly interact with ISWI family chromatin remodelers and thereby regulate remodeling activities. It is known that acetylation of H4 lysine 16 inhibits the activity of ISWI *in vitro*<sup>56</sup>. In addition, bromodomain PHD finger transcription factor (BPTF) sub-unit of the human NURF complex recognizes two different histone modifications, with the PHD finger binds H3K4me3 and the adjacent bromodomain binding acetylated H4K12, 14 or 16 (ref. 69). Furthermore, the chromodomains of human Chd1 recognize H3K4me3<sup>70-72</sup>. It is believed that these modifications target chromatin remodelers to specific chromatin regions to regulate gene transcription. Although it remains to be established that H3K56ac directly recruits remodelers, our data show that the H3K56ac mark stimulates ISW1 activity, both *in vitro* and *in vivo*, revealing a mechanism for regulating chromatin remodeling of nascent chromatin following DNA replication.

### H3K56 deacetylation signals the completion of chromatin maturation

One of the unresolved questions in chromatin remodeling is how chromatin remodelers know to stop chromatin remodeling. It was proposed that some chromatin remodelers can sense linker length between nucleosomes, as a short nucleosome linker length inhibits the activity of chromatin remodelers<sup>67</sup>. In nascent chromatin following DNA replication, we suggest that removal of H3K56ac can provide another signal to reduce action of chromatin remodelers. Supporting this idea, we found that deletion of *HST3* and *HST4* in either wild type

or *mcm2-3A* cells results in an increase in nucleosome repeat length and a reduction of closely-packed nucleosomes at both leading and lagging strands compared to the corresponding wild type or *mcm2-3A* cells. Hst4 removes H3K56ac during G2/M phase of the cell cycle<sup>34,35</sup>. In the absence of *HST3* and *HST4*, over 90% of histone H3 proteins contain H3K56ac. These results indicate that the presence of H3K56ac after S phase will inhibit chromatin maturation, which is likely due to continued chromatin remodeling. Interestingly, deletion of *CHD1* or *ISW1* partially suppresses the sensitivity of *hst3Δ hst4Δ* cells towards to HU and CPT, suggesting that unregulated chromatin remodeling has a negative impact on overall fitness in the presence of these environmental stressors. Together, these results indicate that chromatin remodelers collaborate with H3K56ac to promote the restoration of the phased nucleosome array, and H3K56ac removal after S phase is important for the completion of chromatin maturation.

While we have shown that H3K4me3 is unlikely the driver for chromatin maturation, it is known that parental histones can memorize their positions along the DNA<sup>16,17</sup>. In the absence of both Dpb3 and Mcm2 that compromises parental histone transfer to both leading and lagging strands, parental nucleosomes fail to recover their positions<sup>16</sup>. Therefore, it is possible that the positions of parental nucleosomes also provide a signal to chromatin remodelers on the completion of nascent chromatin maturation. Furthermore, in addition to H3K56ac, newly synthesized histones H3-H4 is also marked by acetylation of lysine 5 and 12 of histone H4<sup>73,74</sup> and un-methylated H4K20 (ref. 75). H4K5,12ac has been linked to histone import, and H4K20me0 is linked to DNA repair. It would be interesting also to determine whether these modifications characteristic of newly synthesized histones have a role in chromatin maturation.

## Methods

### Strains and plasmids

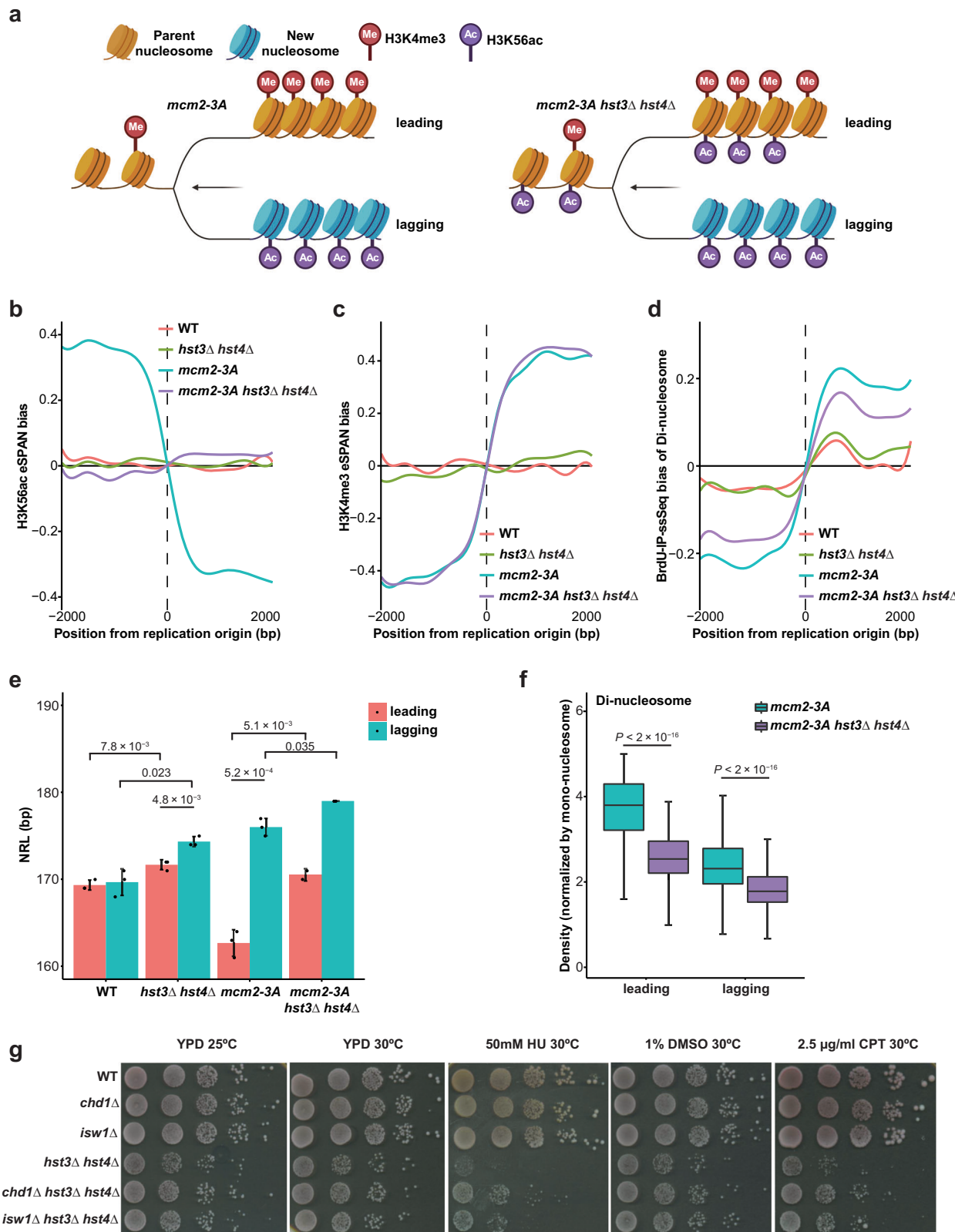
All yeast strains utilized in this study share a W303-1A derived haploid genetic background (*MATa leu2-3, 112 ura3-1 his3-11,15 trp1-1, ade2-1 can1-100*) and are detailed in Supplementary Table 1. The plasmid pRS313/(*H3K56R*) was used to generate the *H3K56R* mutation by replacing the plasmid pWZ414/(*H3WT*) in the yeast strain ZGY1074.

### Yeast culture conditions

Yeast cells were synchronized and cultured following the standard protocol<sup>76</sup>. They were grown in rich medium (1% yeast extract, 2% peptone) supplemented with 2% glucose (YPD) at 30 °C. Exponentially growing cells were arrested at the G1 phase with 5 µg/ml alpha-factor (EZBiolab) for 3 hours in YPD medium at 25 °C when the OD<sub>600</sub> reached 0.4-0.5. Prior to completion, cell morphology was monitored to ensure the G1 arrest (bar-shaped).

### Chromatin immunoprecipitation (ChIP)

Arrested cells were collected by centrifugation, washed twice with cold H<sub>2</sub>O, and then released into fresh medium (YPD) at 25 °C with 400 µg/ml BrdU (B5002, Sigma, see details in Supplementary Data 1). For time-course experiments, exponentially growing cells in YPD were arrested



at G1 using alpha-factor as previously described. Subsequently, 3.15 mg/ml thymidine (T1895, Sigma) was added 30 minutes after release to prevent further BrdU incorporation. At the specified time points (30, 60, and 90 minutes after release), 50 ml of culture were cross-linked with 1% paraformaldehyde for 20 minutes at room temperature, then quenched with 125 mM glycine for 5 minutes at room temperature. For cells with *RTT109*, *CHD1*, or *ISW1* deletion, or the

*H3K56R* mutation, freshly prepared paraformaldehyde was added 30 minutes after release. For samples lacking Hst3 and Hst4, cross-linking was performed 45 minutes after release. The cells were collected by centrifugation, resuspended in ChIP lysis buffer (50 mM HEPES/KOH pH 7.5, 1% Triton X-100, 0.1% Na-deoxycholate, 140 mM NaCl, 1 mM EDTA, and 1x SIGMAFAST Protease Inhibitor Cocktail (S8830, Sigma-Aldrich)), and lysed using glass beads.

**Fig. 6 | Persistent H3K56ac in *hst3Δ hst4Δ* cells results in increased nucleosome repeat length, contributing to genome instability.** **a** A model depicting that H3K56ac, a mark on newly synthesized H3, could be detected on both parental and newly synthesized H3 in *mcm2-3A hst3Δ hst4Δ* cells. **b** and **c** Average bias of H3K56ac (**b**) and H3K4me3 (**c**) eSPAN bias within 4 kb of 134 early-firing replication in indicated yeast strains. **d** Average BrdU-IP-ssSeq bias of di-nucleosomes within 4 kb of 134 early-firing replication origins at indicated yeast strains. **e** Bar plot quantification of the NRL at leading and lagging strands in WT, *hst3Δ hst4Δ*, *mcm2-3A*, and *mcm2-3A hst3Δ hst4Δ* cells. The number of independent repeats of BrdU-IP-ssSeq for WT, *hst3Δ hst4Δ*, *mcm2-3A*, and *mcm2-3A hst3Δ hst4Δ* is 3, 3, 3, and 2, respectively. P values were calculated with two-sided Student's t-test was performed. Data were presented as mean values  $\pm$  standard deviation; error bars

represent standard deviation. **f** Box plots of di-nucleosome density across the early replicated genes shared by three yeast strains (replicated genes = 1398). Density is normalized by mono-nucleosome levels. Box plots show the median, 25% and 75% quartiles and minimal and maximal values. P values were calculated using two-sided Mann-Whitney-Wilcoxon tests. **g** Depletion of *ISW1* and *CHD1* partially suppresses DNA damage sensitivity of *hst3Δ hst4Δ* mutant cells. Ten-fold diluted yeast cells of the indicated genotype on the left were spotted onto YPD medium alone or YPD medium supplemented with hydroxyurea (HU), dimethyl sulfoxide (DMSO), or camptothecin (CPT). For **e** and **f**, source data are provided as a Source Data file. Schematic in **a** was created in BioRender. Zhou, H. (2024) <https://BioRender.com/d28x330>.

To carry out ChIP for H3K4me3 and H3K56ac, chromatin was pelleted and washed twice with NP buffer (1.6 M sorbitol, 5 mM MgCl<sub>2</sub>, 50 mM NaCl, 2 mM CaCl<sub>2</sub>, 14 mM  $\beta$ -mercaptoethanol, 0.075% NP-40, 10 mM Tris-HCl (pH 7.4), 5 mM spermidine). The chromatin was then resuspended in the same buffer and digested with 4U MNase (9013-53-0, Worthington Biochemical) for 20 minutes at 37 °C, resulting in primarily mono- and di-nucleosome fragments. The digestion was terminated by adding 5  $\mu$ l of 0.5 M EDTA and 1/5 volume of 5x ChIP lysis buffer, followed by incubation on ice for at least 30 minutes.

Following MNase digestion, the chromatin was cleared by centrifugation and then immunoprecipitated using specific antibodies (anti-H3K4me3 (300 ng/ $\mu$ l, ab8580, Abcam) and homemade anti-H3K56ac<sup>27</sup> (100 ng/ $\mu$ l)) along with protein G Sepharose beads (17-0618-02, GE Healthcare). The beads were extensively washed, and DNA from both Input and ChIP samples was extracted via the Chelex-100 protocol<sup>27</sup> and utilized for BrdU IP/eSPAN or purified using the MinElute PCR Purification Kit (28004, Qiagen) for ChIP. Subsequently, single-stranded DNA sequencing libraries were constructed with the Accel-NGS 1S Plus DNA Library Kit (10096, Swift Biosciences).

#### BrdU immunoprecipitation (IP) and eSPAN

BrdU immunoprecipitation was performed using either input DNA for BrdU-IP-ssSeq, and H3K4me3 or H3K56ac ChIP DNAs for eSPAN. Briefly, input or ChIP DNA obtained from the Chelex-100 extraction was incubated at 100 °C for 10 minutes and then immediately cooled on ice for 10 minutes. BrdU immunoprecipitation was conducted by diluting the DNA ten-fold with BrdU IP buffer (PBS, 0.0625% Triton X-100 (v/v), 6.7  $\mu$ g/ml Escherichia coli tRNA, 0.17  $\mu$ g/ml BrdU antibody (555627, BD Bioscience)) and rotating for 2 hours at 4 °C. Protein G Sepharose beads were added and incubated for another hour at 4 °C. After extensive washing, the DNA was extracted with 100  $\mu$ l of 1x TE buffer containing 1% SDS at 65 °C for 15 minutes and then eluted again with 50  $\mu$ l of 1x TE buffer containing 1% SDS. The collected supernatants were subsequently purified using the MinElute PCR Purification Kit (Qiagen, 28004). Quantitative PCR was performed to analyze Input, BrdU-IP, ChIP, or eSPAN DNA using primers for the early replication origin ARS607 and the distant site ARS607+14kb<sup>78</sup>. Single-stranded DNA sequencing libraries were prepared using the Accel-NGS 1S Plus DNA Library Kit (10096, Swift Biosciences).

**Purification of yeast ISW1a, ISW1b and human SNF2h complexes**  
ISWI complexes can be purified to near homogeneity by following published procedures<sup>61</sup>. The use of three tandem FLAG epitopes (3x FLAG) fused to the C-terminal part of loc3p and loc2p facilitates the purification of Isw1a and Isw1b complexes as previously described<sup>61</sup>. Briefly, yeast cells (YTT2094 and YTT2092) were cultured in rich media (YPD) to a density of OD600 around 2 and harvested separately by centrifugation. The cell pellet was washed once with H<sub>2</sub>O (containing 4 mM phenylmethylsulfonyl fluoride, 1 mM sodium metabisulfite, and 2 mM dithiothreitol) and once with Buffer H-0.3 (25 mM HEPES-KOH, pH 7.6, 0.5 mM EGTA, 0.1 mM EDTA, 2 mM MgCl<sub>2</sub>, 20% glycerol,

0.02% NP-40, 1 mM dithiothreitol, 0.5 mM Na<sub>2</sub>S<sub>2</sub>O<sub>5</sub>, 1 mM phenylmethylsulfonyl fluoride, 2  $\mu$ M pepstatin A, 0.6  $\mu$ M leupeptin, 2  $\mu$ g of chymostatin/ml, 2 mM benzamidine, 0.3 M KCl). The cell pellet was resuspended in an equal volume of Buffer H-0.3 and a freezer mill (6870, SPEX SamplePrep, USA) with default setting was used to grind yeast cells in liquid nitrogen. The lysate was then centrifuged using a Beckman SW40Ti rotor at 130,000 g for 90 minutes, and the supernatant (whole cell extract) was collected.

FLAG-tagged Isw1a or Isw1b complexes were purified using anti-FLAG M2 agarose beads (#A1205, Sigma, St. Louis, Missouri, USA), as described previously<sup>61</sup> and eluted with 3xFLAG peptide (#F4799, Sigma, St. Louis, Missouri, USA) in Buffer H-0.1 at 4 °C for 30 minutes.

SNF2h (*Homo sapiens*) was purified as previously described<sup>79</sup>. SNF2h was expressed using a modified pET3 expression vector with an N-terminal 6xHis tag in Rosetta DE3 E. coli cells. The cells were grown in 2X LB media and induced with IPTG at an OD600 of ~0.6, followed by expression at 18 °C for 18 hours. After harvesting and lysing the cells, the lysate was clarified and subjected to HisTrap affinity chromatography, with SNF2h eluting between 210 and 300 mM imidazole. The protein was further purified using ion exchange and size exclusion chromatography, with a TEV protease step to remove the His tag. The final purified SNF2h was concentrated, glycerol was added, and the protein was flash-frozen and stored at -80 °C.

#### Nucleosome purification

Nucleosomes used for native gel sliding experiments were reconstituted using the Widom 601 positioning sequence<sup>80</sup> and Xenopus laevis histones with or without acetylated histone H3-K56. The DNA (FAM-80-601-0 and FAM-40-601-40) was generated by PCR, concentrated, and then purified by Prep Cell (Bio-Rad). Histone octamers containing wild type or acetylated histone H3-K56 were purchased from the Histone Source (Colorado State University). Nucleosomes were reconstituted through linear gradient dialysis and purified over a Prep Cell apparatus<sup>81</sup>. Fractions were analyzed by native PAGE, and after selected fractions were pooled and concentrated, glycerol was added to final concentration of 20%. Nucleosome samples were aliquoted, flash frozen in liquid nitrogen and stored at -80°C.

#### Native gel sliding experiments

For sliding experiments, master mixes were prepared that contained purified nucleosomes (40 nM) and either 200 nM HsSNF2h, 200 nM Sclsw1a, or 200 nM Sclsw1b. Sliding buffer contained 20 mM HEPES-KOH, pH 7.5, 100 mM KCl, 5 mM MgCl<sub>2</sub>, 2 mM DTT, 0.1 mg/ml BSA, 5% sucrose. Each master mix was equilibrated at room temperature for 10 mins. Sliding reactions were initiated with ATP addition to a final concentration of 2.5 mM ATP, and at each time point, 1  $\mu$ l of master mix was transferred to a tube containing 7.5  $\mu$ l quench buffer (20 mM Hepes-KOH, pH 7.5, 50 mM KCl, 2 mM DTT, 0.1 mg/ml BSA, 5% sucrose, 12.5 mM EDTA, 0.5  $\mu$ g/ $\mu$ l salmon sperm DNA). Sliding reactions were then resolved on 6% native PAGE gels at 4 °C and 100 V for 2 hours and imaged on a Typhoon scanner.

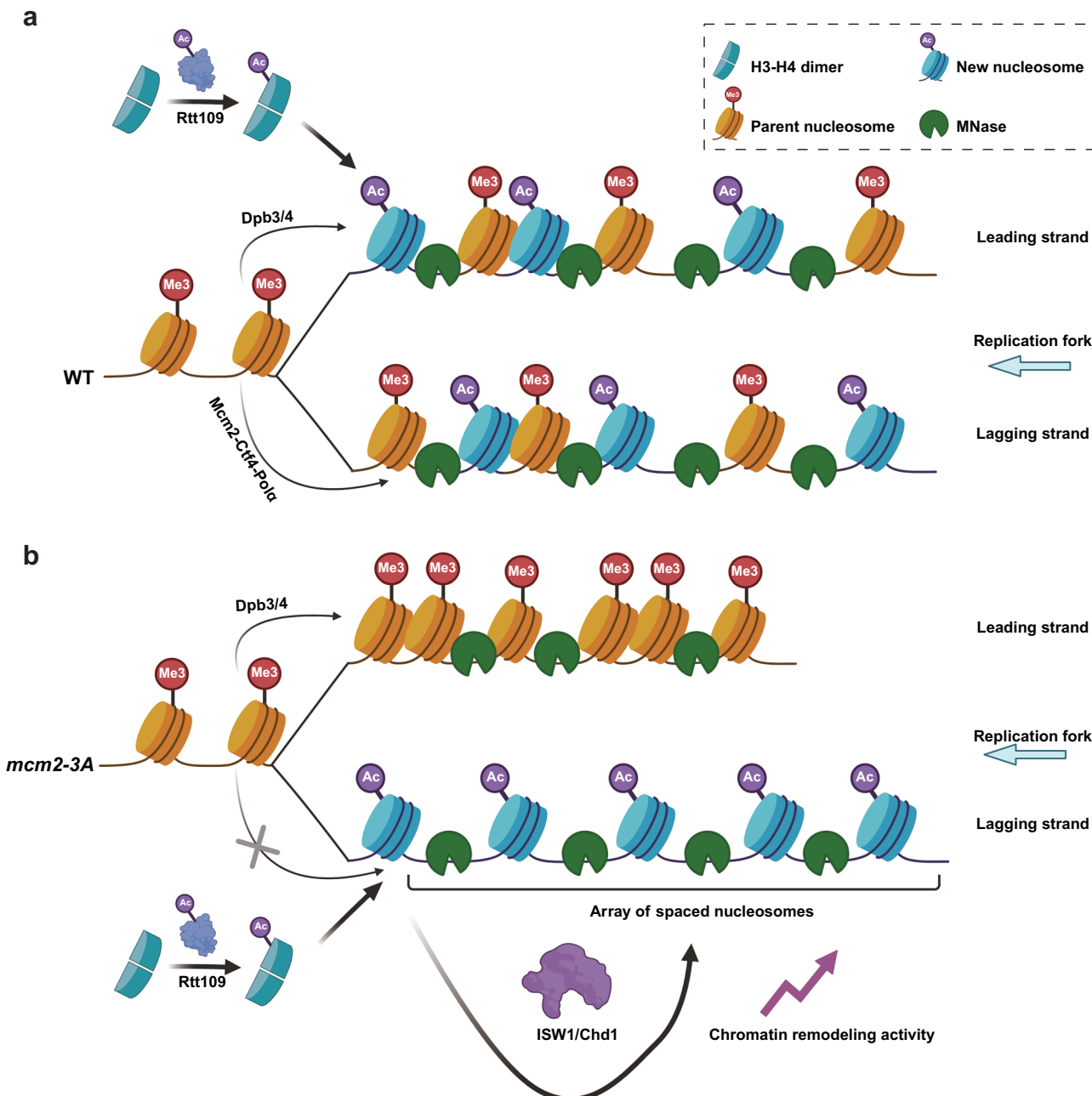


**Fig. 7 | H3K56ac collaborates with the chromatin remodelers Isw1 and Chd1 in chromatin maturation.** Schematic working model. **a** In WT cells, symmetrical distribution of H3K56ac leads to an equal distribution of closely-packed nucleosomes and/or subnucleosomal particles (not depicted here) in nascent chromatin originated from both leading and lagging strand synthesis. **b** In *mcm2-3A* cells, the

enrichment of H3K56ac in nascent chromatin from the lagging strand enhances the chromatin remodeling activity of Isw1 and Chd1, resulting in an extension of the nucleosome repeat length. On the other hand, a reduced levels of H3K56ac at leading strands leads to an increased levels of closely-packed nucleosomes. Created in BioRender. Zhou, H. (2024) <https://BioRender.com/k1998>.

#### MNase-ssSeq, ChIP-seq, BrdU-IP-ssSeq, and eSPAN analysis

**Reads processing and mapping.** Single-stranded DNA sequencing libraries for MNase-ssSeq, ChIP-seq, BrdU-IP-ssSeq, and eSPAN were prepared and then subjected to paired-end sequencing using the Illumina NextSeq 500/550 or NovaSeq 6000 platforms. To improve mapping quality, raw sequencing reads were first processed with Trim Galore (V 0.6.7) to remove low-quality reads and Illumina Prep Kit adaptors. The quality cutoff was set to 20, and the minimum required read length after trimming was 20 nt. The genome sequence and gene annotation for the yeast reference genome (sacCer3) were obtained from SGD (<https://www.yeastgenome.org/>). Paired-end sequencing reads were mapped to yeast genome (sacCer3) using bowtie2

(V 2.2.4)<sup>82</sup> with the following parameters: with --no-mixed --no-discordant --no-dovetail --no-contain --local --maxins 1000.

**Identifying early replicated regions.** Sequence alignment map files, including uniquely mapped, PCR-duplicated, and multi-mapped reads, were transformed into BAM files using SAMtools (V 1.11)<sup>83</sup>. To obtain the accurate mapping reads, duplicate and multi-mapping reads were discarded and only paired-end reads with both ends aligning uniquely to the reference genome were used for further analysis. Duplicate reads were removed using the MarkDuplicates function of Picard (V 2.23.8) (<https://github.com/broadinstitute/picard>) with REMOVE\_DUPLICATES = true. Multi-mapped reads were excluded using SAMtools

(V 1.11) with -q 30 cutoff. The filtered paired-end reads were converted into bigwig files using bamCoverage from deepTools (V 3.2.1)<sup>84</sup> with RPM normalization and 1 bp window size and visualization using Integrative Genomics Viewer (IGV V 2.12.3)<sup>85</sup>. Accurate early-firing region detection was achieved by using filtered paired-end reads of BrdU-IP-ssSeq signals to call broad peaks with MACS2 (V 2.2.5)<sup>86</sup> for each replicate independently, applying a q-value cutoff of 0.001 and using the corresponding MNase-ssSeq Input samples as controls. The peak overlap analysis was performed using the findOverlapsOfPeaks function from ChIPpeakAnno (V 3.18.2)<sup>87</sup>. Only reproducible peaks were retained. The early replicated regions were defined as the BrdU peaks that overlapped with one of the 134 early-firing origins detected in a previous study<sup>13</sup>. The precise nucleosome positions and transcription start site (TSS) locations in yeast, resolved at the base-pair level, were obtained from prior publications.<sup>88,89</sup> The replicated genes and nucleosomes within the replicated regions were selected using the intersect function of BEDtools (V 2.29.2)<sup>90</sup>.

**Calculating BrdU-IP-ssSeq and eSPAN strand bias.** To calculate BrdU-IP-ssSeq and eSPAN strand bias, the filtered paired-end reads aligned to the Watson (W) and Crick (C) strands of the reference genome were partitioned using the bamtobed function of BEDTools (V 2.29.2) and custom Perl scripts. BrdU-IP-ssSeq and eSPAN bias was determined in 10 bp bin from the segregated Watson and Crick reads using the formula Bias= (W - C)/(W + C) across the replicated regions. Bins with fewer than 10 sequencing reads were excluded. The eSPAN bias was furthermore normalized using the corresponding BrdU-IP-ssSeq strand bias, as previously described<sup>54</sup>.

Considering the distribution of fragments and findings from prior research<sup>91</sup>, we classified chromatin fragments into mono-nucleosomes (120-200 bp) and di-nucleosomes (250-400 bp) based on fragment size using custom Perl scripts. Subsequently, the strand bias of mono-nucleosomes and di-nucleosomes of BrdU-IP-ssSeq samples were calculated using the same formula as described above. Taking into account the effect of DNA synthesis on nucleosome assembly, we also normalized the BrdU-IP-ssSeq strand bias calculations from MNase digestion samples against those from sonication samples, whenever corresponding sonication samples were available to mitigate the baseline bias of DNA synthesis.

### Nucleosome occupancy and eSPAN signal

For BrdU-IP-ssSeq and eSPAN reads, we separated the leading strand reads and the lagging strand reads based on the detected replicated regions using BEDTools (V 2.29.2). Paired-end reads from the common replicated regions were used for comparing nucleosome occupancy and eSPAN signals between different samples. In order to visualize the signal change of eSPAN between the leading and lagging strands, plotHeatmap and plotProfile from deepTools to display the eSPAN signal around each of the 134 early replication origins and the average eSPAN signal to describe the changes of eSPAN signal in replicated regions more clearly. For mono-nucleosome occupancy, nucleosomes were enriched and smoothed using the nucleR (V 2.36.0)<sup>92</sup> with the parameters maxfrag = 200 and trimtolength = 50. Di-nucleosomes were split into two mono-nucleosomes from their center, then processed with DANPOS (V 2.2.2)<sup>93</sup> to calculate the average read density flanking a group of TSS or +1 nucleosomes. Boxplot for nucleosome occupancy was used to visualize the quantification results in replicated regions.

### Nucleosome repeat length analysis

Following previous approach<sup>50,94</sup>, we extracted and unified the 5'-end positions of unshifted MNase alignments in replicated regions. The calcPhasogram function from the swissknife package (<https://github.com/fmicompbio/swissknife>) was used to calculate the frequencies of same-strand alignment distances between nearby positions on the

same strand (up to 1000 bp), which were visualized using plotPhasogram. The estimateNRL function estimated nucleosome repeat length from the frequencies of alignment distances: distances between 75 and 1000 bp were smoothed twice using loess (span=0.1 and span=1.5). Differences between the smoothed counts were computed, and the first three modes were identified. The nucleosome repeat length was derived from the slope of a linear fit of the mode indices 1, 2, and 3 (corresponding to the mono-, di-, and tri-nucleosome fragment lengths) to the distances at which these modes were observed.

### Nucleosome sliding rate analysis

Bands representing different nucleosome species were quantitated using ImageJ<sup>95</sup>, and rates of appearance of centered bands were calculated based on fitting to a single exponential. The fitting and plotting were all conducted using a Python program. The progress curves were fitted to the equation  $y = A(1 - \exp(k*t)) + c$ , where A is amplitude, k is the rate, and c is a constant that accounts for curves not starting exactly at zero.

### Statistics and reproducibility

A total of 2-4 biological replicates were done for MNase-ssSeq, ChIP-seq, BrdU-IP-ssSeq, and eSPAN. 5-7 biological replicates were done for nucleosome sliding and processivity assays as indicated. Nucleosome repeat length data were presented as bar plots showing the mean  $\pm$  standard deviation. In the figures of the nucleosome density data, box plots were created using R 3.6.3 and depict the medians and interquartile ranges (IQRs), with upper and lower whiskers. The boundaries of the box indicate values from the first quartile (Q1) to the third quartile (Q3) (25% to 75%). The center line within the box represents the median value. The IQR is defined as the distance between Q3 and Q1 (Q3 - Q1). The upper whisker extends to the maximum value, which is defined as 1.5 times the IQR above Q3 (Q3 + 1.5  $\times$  IQR), while the lower whisker extends to the minimum value, defined as 1.5 times the IQR below Q1 (Q1 - 1.5  $\times$  IQR). Outliers were omitted from the box plots for clarity but were still considered in the calculation of P values. Where applicable, statistical parameters, the tests used, definitions of error bars, and sample sizes are reported in the figures and their corresponding legends.

### Reporting summary

Further information on research design is available in the Nature Portfolio Reporting Summary linked to this article.

### Data availability

The raw and processed high-throughput sequencing data discussed in this study have been deposited in NCBI's Gene Expression Omnibus and are accessible through GEO Series accession number [GSE269558](https://www.ncbi.nlm.nih.gov/geo/query/acc.cgi?acc=GSE269558). All other data supporting the findings are available within the article and its supplementary files. Requests for additional information can be directed to the corresponding authors. Source data are provided with this paper.

### References

1. Luger, K., Mader, A. W., Richmond, R. K., Sargent, D. F. & Richmond, T. J. Crystal structure of the nucleosome core particle at 2.8 Å resolution. *Nature* **389**, 251–260 (1997).
2. Ransom, M., Dennehey, B. K. & Tyler, J. K. Chaperoning histones during DNA replication and repair. *Cell* **140**, 183–195 (2010).
3. Margueron, R. & Reinberg, D. Chromatin structure and the inheritance of epigenetic information. *Nat. Rev. Genet.* **11**, 285–296 (2010).
4. Serra-Cardona, A. & Zhang, Z. Replication-coupled nucleosome assembly in the passage of epigenetic information and cell identity. *Trends Biochem. Sci.* **43**, 136–148 (2018).
5. Moazed, D. Mechanisms for the inheritance of chromatin states. *Cell* **146**, 510–518 (2011).

6. Groth, A., Rocha, W., Verreault, A. & Almouzni, G. Chromatin challenges during DNA replication and repair. *Cell* **128**, 721–733 (2007).
7. Wu, G. et al. Somatic histone H3 alterations in pediatric diffuse intrinsic pontine gliomas and non-brainstem glioblastomas. *Nat. Genet.* **44**, 251–253 (2012).
8. Chan, K. M. et al. The histone H3.3K27M mutation in pediatric glioma reprograms H3K27 methylation and gene expression. *Genes Dev.* **27**, 985–990 (2013).
9. Lewis, P. W. & Allis, C. D. Poisoning the “histone code” in pediatric gliomagenesis. *Cell Cycle* **12**, 3241–3242 (2013).
10. Plass, C. et al. Mutations in regulators of the epigenome and their connections to global chromatin patterns in cancer. *Nat. Rev. Genet.* **14**, 765–780 (2013).
11. Lesch, B. J. et al. Intergenerational epigenetic inheritance of cancer susceptibility in mammals. *eLife* **8**, e39380 (2019).
12. Parreno, V. et al. Transient loss of Polycomb components induces an epigenetic cancer fate. *Nature* **629**, 688–696 (2024).
13. Yu, C. H. et al. A mechanism for preventing asymmetric histone segregation onto replicating DNA strands. *Science* **361**, 1386–1389 (2018).
14. Gan, H. et al. The Mcm2-Ctf4-Pol $\alpha$  Axis Facilitates Parental Histone H3-H4 Transfer to Lagging Strands. *Mol. Cell* **72**, 140–151.e3 (2018).
15. Petryk, N. et al. MCM2 promotes symmetric inheritance of modified histones during DNA replication. *Science* **361**, 1389–1392 (2018).
16. Schlissel, G. & Rine, J. The nucleosome core particle remembers its position through DNA replication and RNA transcription. *Proc. Natl. Acad. Sci. USA* **116**, 20605–20611 (2019).
17. Escobar, T. M. et al. Active and repressed chromatin domains exhibit distinct nucleosome segregation during DNA replication. *Cell* **179**, 953–963 (2019).
18. Gan, H. et al. The Mcm2-Ctf4-Pol $\alpha$  axis facilitates parental histone H3-H4 transfer to lagging strands. *Mol. Cell* **72**, 140–151 (2018).
19. Serra-Cardona, A. et al. The PCNA-Pol $\delta$  complex couples lagging strand DNA synthesis to parental histone transfer for epigenetic inheritance. *Sci. Adv.* **10**, eadn5175 (2024).
20. English, C. M., Adkins, M. W., Carson, J. J., Churchill, M. E. & Tyler, J. K. Structural basis for the histone chaperone activity of Asf1. *Cell* **127**, 495–508 (2006).
21. Li, Q. et al. Acetylation of histone H3 lysine 56 regulates replication-coupled nucleosome assembly. *Cell* **134**, 244–255 (2008).
22. Burgess, R. J., Zhou, H., Han, J. & Zhang, Z. A role for Gcn5 in replication-coupled nucleosome assembly. *Mol. Cell* **37**, 469–480 (2010).
23. Campos, E. I. et al. The program for processing newly synthesized histones H3.1 and H4. *Nat. Struct. Mol. Biol.* **17**, 1343–1351 (2010).
24. Su, D. et al. Structural basis for recognition of H3K56-acetylated histone H3-H4 by the chaperone Rtt106. *Nature* **483**, 104–107 (2012).
25. Chen, C. C. et al. Acetylated lysine 56 on histone H3 drives chromatin assembly after repair and signals for the completion of repair. *Cell* **134**, 231–243 (2008).
26. Han, J. et al. A Cul4 E3 ubiquitin ligase regulates histone hand-off during nucleosome assembly. *Cell* **155**, 817–829 (2013).
27. Han, J. et al. Rtt109 acetylates histone H3 lysine 56 and functions in DNA replication. *Science* **315**, 653–655 (2007).
28. Collins, S. R. et al. Functional dissection of protein complexes involved in yeast chromosome biology using a genetic interaction map. *Nature* **446**, 806–810 (2007).
29. Han, J., Zhou, H., Li, Z., Xu, R. M. & Zhang, Z. The Rtt109-Vps75 histone acetyltransferase complex acetylates non-nucleosomal histone H3. *J. Biol. Chem.* **282**, 14158–14164 (2007).
30. Han, J., Zhou, H., Li, Z., Xu, R. M. & Zhang, Z. Acetylation of lysine 56 of histone H3 catalyzed by Rtt109 and regulated by Asf1 is required for replisome integrity. *J. Biol. Chem.* **282**, 28587–28596 (2007).
31. Winkler, D. D., Zhou, H., Dar, M. A., Zhang, Z. & Luger, K. Yeast CAF-1 assembles histone (H3-H4)2 tetramers prior to DNA deposition. *Nucleic Acids Res.* **40**, 10139–10149 (2012).
32. Fazly, A. et al. Histone chaperone Rtt106 promotes nucleosome formation using (H3-H4)2 tetramers. *J. Biol. Chem.* **287**, 10753–10760 (2012).
33. Liu, C. P. et al. Structural insights into histone binding and nucleosome assembly by chromatin assembly factor-1. *Science* **381**, 850–850+ (2023).
34. Maas, N. L., Miller, K. M., DeFazio, L. G. & Toczyński, D. P. Cell cycle and checkpoint regulation of histone H3 K56 acetylation by Hst3 and Hst4. *Mol. Cell* **23**, 109–119 (2006).
35. Celic, I. et al. The sirtuins Hst3 and Hst4p preserve genome integrity by controlling histone H3 lysine 56 deacetylation. *Curr. Biol.* **16**, 1280–1289 (2006).
36. Gutierrez, M. P., MacAlpine, H. K. & MacAlpine, D. M. Nascent chromatin occupancy profiling reveals locus- and factor-specific chromatin maturation dynamics behind the DNA replication fork. *Genome Res.* **29**, 1123–1133 (2019).
37. Ramachandran, S. & Henikoff, S. Transcriptional regulators compete with nucleosomes post-replication. *Cell* **165**, 580–592 (2016).
38. Vasseur, P. et al. Dynamics of nucleosome positioning maturation following genomic replication. *Cell Rep.* **16**, 2651–2665 (2016).
39. Clapier, C. R., Iwasa, J., Cairns, B. R. & Peterson, C. L. Mechanisms of action and regulation of ATP-dependent chromatin-remodelling complexes. *Nat. Rev. Mol. Cell Biol.* **18**, 407–422 (2017).
40. Zhou, C. Y., Johnson, S. L., Gamarra, N. I. & Narlikar, G. J. Mechanisms of ATP-dependent chromatin remodeling motors. *Annu. Rev. Biophys.* **45**, 153–181 (2016).
41. Lusser, A. & Kadonaga, J. T. Chromatin remodeling by ATP-dependent molecular machines. *Bioessays* **25**, 1192–1200 (2003).
42. Morrison, A. J. & Shen, X. Chromatin remodelling beyond transcription: the INO80 and SWR1 complexes. *Nat. Rev. Mol. Cell Biol.* **10**, 373–384 (2009).
43. Ito, T., Bulger, M., Pazin, M. J., Kobayashi, R. & Kadonaga, J. T. ACF, an ISWI-containing and ATP-utilizing chromatin assembly and remodeling factor. *Cell* **90**, 145–155 (1997).
44. Torigoe, S. E., Urwin, D. L., Ishii, H., Smith, D. E. & Kadonaga, J. T. Identification of a rapidly formed nonnucleosomal histone-DNA intermediate that is converted into chromatin by ACF. *Mol. Cell* **43**, 638–648 (2011).
45. Tsukiyama, T., Daniel, C., Tamkun, J. & Wu, C. ISWI, a member of the SWI2/SNF2 ATPase family, encodes the 140 kDa subunit of the nucleosome remodeling factor. *Cell* **83**, 1021–1026 (1995).
46. Tsukiyama, T., Palmer, J., Landel, C. C., Shiloch, J. & Wu, C. Characterization of the imitation switch subfamily of ATP-dependent chromatin-remodeling factors in *Saccharomyces cerevisiae*. *Genes Dev.* **13**, 686–697 (1999).
47. Ocampo, J., Chereji, R. V., Eriksson, P. R. & Clark, D. J. The ISW1 and CHD1 ATP-dependent chromatin remodelers compete to set nucleosome spacing. *Nucleic Acids Res.* **44**, 4625–4635 (2016).
48. Eriksson, P. R. & Clark, D. J. The yeast ISW1b ATP-dependent chromatin remodeler is critical for nucleosome spacing and dinucleosome resolution. *Sci. Rep.* **11**, 4195 (2021).
49. Bhardwaj, S. K. et al. Dinucleosome specificity and allosteric switch of the ISW1a ATP-dependent chromatin remodeler in transcription regulation. *Nat. Commun.* **11**, 5913 (2020).
50. Bomber, M. L. et al. Human SMARCA5 is continuously required to maintain nucleosome spacing. *Mol. Cell* **83**, 507–522 (2023).
51. Noll, M. Subunit structure of chromatin. *Nature* **251**, 249–251 (1974).
52. Yu, C. et al. Strand-specific analysis shows protein binding at replication forks and PCNA unloading from lagging strands when forks stall. *Mol. Cell* **56**, 551–563 (2014).

53. Song, F. et al. Cryo-EM study of the chromatin fiber reveals a double helix twisted by tetranucleosomal units. *Science* **344**, 376–380 (2014).

54. Serra-Cardona, A., Duan, S. F., Yu, C. H. & Zhang, Z. G. H3K4me3 recognition by the COMPASS complex facilitates the restoration of this histone mark following DNA replication. *Sci. Adv.* **8**, eabm6246 (2022).

55. Weiner, A. et al. High-resolution chromatin dynamics during a yeast stress response. *Mol. Cell* **58**, 371–386 (2015).

56. Shogren-Knaak, M. et al. Histone H4-K16 acetylation controls chromatin structure and protein interactions. *Science* **311**, 844–847 (2006).

57. Shilatifard, A. The COMPASS family of histone H3K4 methylases: mechanisms of regulation in development and disease pathogenesis. *Annu. Rev. Biochem.* **81**, 65–95 (2012).

58. Ocampo, J., Chereji, R. V., Eriksson, P. R. & Clark, D. J. Contrasting roles of the RSC and ISWI/CHD1 chromatin remodelers in RNA polymerase II elongation and termination. *Genome Res.* **29**, 407–417 (2019).

59. Chacin, E. et al. Establishment and function of chromatin organization at replication origins. *Nature* **616**, 836–842 (2023).

60. Neumann, H. et al. A method for genetically installing site-specific acetylation in recombinant histones defines the effects of H3 K56 acetylation. *Mol. Cell* **36**, 153–163 (2009).

61. Vary, J. C. et al. Yeast Isw1p forms two separable complexes in vivo. *Mol. Cell. Biol.* **23**, 80–91 (2003).

62. Stockdale, C., Flaus, A., Ferreira, H. & Owen-Hughes, T. Analysis of nucleosome repositioning by yeast ISWI and Chd1 chromatin remodeling complexes. *J. Biol. Chem.* **281**, 16279–16288 (2006).

63. Li, Y. A. et al. The emerging role of ISWI chromatin remodeling complexes in cancer. *J. Exp. Clin. Cancer Res.* **40**, 346 (2021).

64. Dann, G. P. et al. ISWI chromatin remodelers sense nucleosome modifications to determine substrate preference. *Nature* **548**, 607–611 (2017).

65. Engeholm, M. et al. Resolution of transcription-induced hexasome-nucleosome complexes by Chd1 and FACT. *Mol. Cell* **84**, 3423–3437.e8 (2024).

66. Li, Z. et al. DNA polymerase  $\alpha$  interacts with H3-H4 and facilitates the transfer of parental histones to lagging strands. *Sci. Adv.* **6**, eabb5820 (2020).

67. Li, L. et al. Structure of the ISW1a complex bound to the dinucleosome. *Nat. Struct. Mol. Biol.* **31**, 266–274 (2024).

68. Park, S., Brandani, G. B., Ha, T. & Bowman, G. D. Bi-directional nucleosome sliding by the Chd1 chromatin remodeler integrates intrinsic sequence-dependent and ATP-dependent nucleosome positioning. *Nucleic Acids Res.* **51**, 10326–10343 (2023).

69. Ruthenburg, A. J. et al. Recognition of a mononucleosomal histone modification pattern by BPTF via multivalent interactions. *Cell* **145**, 692–706 (2011).

70. Pray-Grant, M. G., Daniel, J. A., Schieltz, D. & Yates, J. R. 3rd & Grant, P. A. Chd1 chromodomain links histone H3 methylation with SAGA- and SLIK-dependent acetylation. *Nature* **433**, 434–438 (2005).

71. Flanagan, J. F. et al. Double chromodomains cooperate to recognize the methylated histone H3 tail. *Nature* **438**, 1181–1185 (2005).

72. Sims, R. J. 3rd et al. Human but not yeast CHD1 binds directly and selectively to histone H3 methylated at lysine 4 via its tandem chromodomains. *J. Biol. Chem.* **280**, 41789–41792 (2005).

73. Sobel, R. E., Cook, R. G., Perry, C. A., Annunziato, A. T. & Allis, C. D. Conservation of deposition-related acetylation sites in newly synthesized histones H3 and H4. *Proc. Natl Acad. Sci. USA* **92**, 1237–1241 (1995).

74. Zhang, H., Han, J., Kang, B., Burgess, R. & Zhang, Z. Human histone acetyltransferase 1 protein preferentially acetylates H4 histone molecules in H3.1-H4 over H3.3-H4. *J. Biol. Chem.* **287**, 6573–6581 (2012).

75. Saredi, G. et al. H4K20me0 marks post-replicative chromatin and recruits the TONSL-MMS22L DNA repair complex. *Nature* **534**, 714–718 (2016).

76. Dunham, M. J., Gartenberg, M. R. & Brown, G. W. Methods in yeast genetics and genomics: a laboratory course manual. Cold Spring Harbor Laboratory Press, xvii, 233 pages (2015).

77. Nelson, J. D., Denisenko, O. & Bomsztyk, K. Protocol for the fast chromatin immunoprecipitation (ChIP) method. *Nat. Protoc.* **1**, 179–185 (2006).

78. Han, J. H. et al. Ubiquitylation of FACT by the Cullin-E3 ligase Rtt101 connects FACT to DNA replication. *Genes Dev.* **24**, 1485–1490 (2010).

79. Levendosky, R. F. & Bowman, G. D. Asymmetry between the two acidic patches dictates the direction of nucleosome sliding by the ISWI chromatin remodeler. *eLife* **8**, e45472 (2019).

80. Lowary, P. T. & Widom, J. New DNA sequence rules for high affinity binding to histone octamer and sequence-directed nucleosome positioning. *J. Mol. Biol.* **276**, 19–42 (1998).

81. Nodelman, I. M., Patel, A., Levendosky, R. F. & Bowman, G. D. Reconstitution and purification of nucleosomes with recombinant histones and purified DNA. *Curr. Protoc. Mol. Biol.* **133**, e130 (2020).

82. Langmead, B. & Salzberg, S. L. Fast gapped-read alignment with Bowtie 2. *Nat. Methods* **9**, 357–359 (2012).

83. Danecek, P. et al. Twelve years of SAMtools and BCFtools. *Giga-science* **10**, 1–4 (2021).

84. Ramirez, F. et al. deepTools2: a next generation web server for deep-sequencing data analysis. *Nucleic Acids Res.* **44**, W160–W165 (2016).

85. Robinson, J. T. et al. Integrative genomics viewer. *Nat. Biotechnol.* **29**, 24–26 (2011).

86. Feng, J. X., Liu, T., Qin, B., Zhang, Y. & Liu, X. S. Identifying ChIP-seq enrichment using MACS. *Nat. Protoc.* **7**, 1728–1740 (2012).

87. Zhu, L. J. et al. ChIPpeakAnno: a Bioconductor package to annotate ChIP-seq and ChIP-chip data. *BMC Bioinforma.* **11**, 237 (2010).

88. Brogaard, K., Xi, L. Q., Wang, J. P. & Widom, J. A map of nucleosome positions in yeast at base-pair resolution. *Nature* **486**, 496–501 (2012).

89. Bagchi, D. N., Battenhouse, A. M., Park, D. & Iyer, V. R. The histone variant H2A.Z in yeast is almost exclusively incorporated into the +1 nucleosome in the direction of transcription. *Nucleic Acids Res.* **48**, 157–170 (2020).

90. Quinlan, A. R. & Hall, I. M. BEDTools: a flexible suite of utilities for comparing genomic features. *Bioinformatics* **26**, 841–842 (2010).

91. Schwartz, U. et al. Characterizing the nuclelease accessibility of DNA in human cells to map higher order structures of chromatin. *Nucleic Acids Res.* **47**, 1239–1254 (2019).

92. Flores, O. & Orozco, M. nucleR: a package for non-parametric nucleosome positioning. *Bioinformatics* **27**, 2149–2150 (2011).

93. Chen, K. F. et al. DANPOS: Dynamic analysis of nucleosome position and occupancy by sequencing. *Genome Res.* **23**, 341–351 (2013).

94. Barisic, D., Stadler, M. B., Iurlaro, M. & Schubeler, D. Mammalian ISWI and SWI/SNF selectively mediate binding of distinct transcription factors. *Nature* **569**, 136–140 (2019).

95. Schneider, C. A., Rasband, W. S. & Eliceiri, K. W. NIH image to ImageJ: 25 years of image analysis. *Nat. Methods* **9**, 671–675 (2012).

## Acknowledgements

We thank Robert Levendosky for purified SNF2h protein. We also thank Drs. Richard Baer and Songtao Jia for critical reading and editing of the manuscript. This study was supported by R35GM118015 (to Z.Z.), R01GM084192 (to G.D.B.), and R35GM139429 (to T.T.). This study used resources (high-throughput sequencing) at Herbert Irving Comprehensive Cancer Center (HICCC) funded in part through NIH/NCI Cancer Center Support Grant P30CA013696.

## Author contributions

S.D. and Z.Z. conceived and supervised the project. S.D. performed most of the experiments and the bioinformatic analysis. I.M.N. performed nucleosome sliding assay experiment. H.Z. prepared CUT&RUN libraries. T.T. provided yeast strains and supervised yeast Isw1a and Isw1b purification. G.D.B. supervised human SNF2h purification and nucleosome sliding assay experiments. S.D. and Z.Z. prepared the figures and wrote the manuscript. All authors read and edited the paper.

## Competing interests

The authors declare no competing interests.

## Additional information

**Supplementary information** The online version contains supplementary material available at <https://doi.org/10.1038/s41467-024-55144-7>.

**Correspondence** and requests for materials should be addressed to Shoufu Duan or Zhiguo Zhang.

**Peer review information** *Nature Communications* thanks the anonymous reviewers for their contribution to the peer review of this work. A peer review file is available.

**Reprints and permissions information** is available at <http://www.nature.com/reprints>

**Publisher's note** Springer Nature remains neutral with regard to jurisdictional claims in published maps and institutional affiliations.

**Open Access** This article is licensed under a Creative Commons Attribution-NonCommercial-NoDerivatives 4.0 International License, which permits any non-commercial use, sharing, distribution and reproduction in any medium or format, as long as you give appropriate credit to the original author(s) and the source, provide a link to the Creative Commons licence, and indicate if you modified the licensed material. You do not have permission under this licence to share adapted material derived from this article or parts of it. The images or other third party material in this article are included in the article's Creative Commons licence, unless indicated otherwise in a credit line to the material. If material is not included in the article's Creative Commons licence and your intended use is not permitted by statutory regulation or exceeds the permitted use, you will need to obtain permission directly from the copyright holder. To view a copy of this licence, visit <http://creativecommons.org/licenses/by-nc-nd/4.0/>.

© The Author(s) 2024